Molecular Cell

Article

Competition between two HUSH complexes orchestrates the immune response to retroelement invasion

Graphical abstract

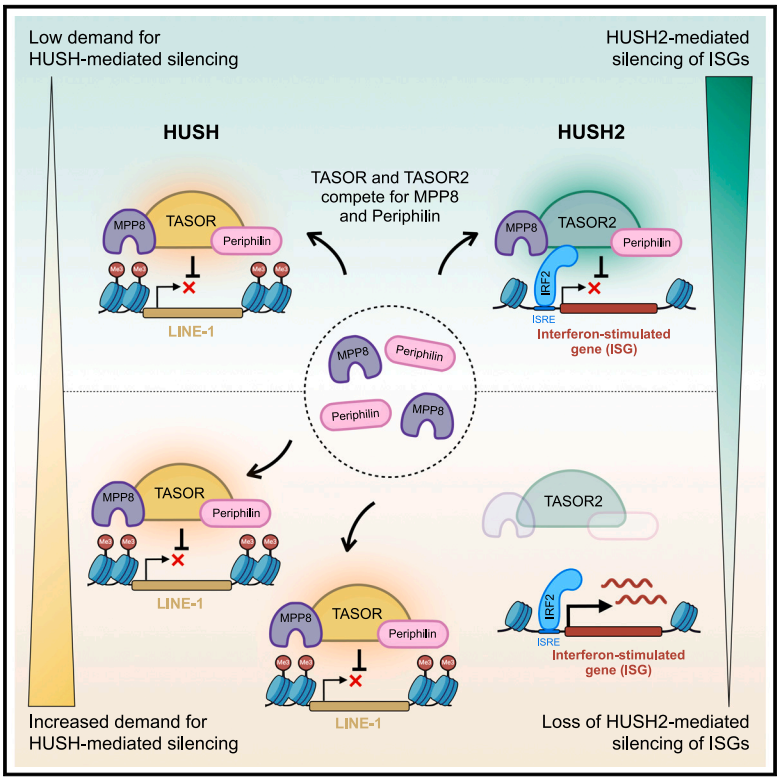

Highlights

- TASOR2 binds MPP8 and Periphilin to form a HUSH2 complex
- An IRF2-TASOR2 interaction recruits HUSH2 to repress interferon-stimulated genes
- TASOR and TASOR2 compete for a limited pool of MPP8 and Periphilin
- Competition between HUSH and HUSH2 couples retroelement silencing to the induction of ISGs

Authors

Joshua Miguel C. Danac, Rachael E. Matthews, Akhila Gungi, ..., Robin Antrobus, Richard T. Timms, Iva A. Tchasovnikarova

Correspondence

it257@cam.ac.uk

In brief

The HUSH complex, composed of TASOR, MPP8, and Periphilin, facilitates epigenetic silencing of retroelements. Danac et al. now describe HUSH2, centered around the TASOR paralog TASOR2, which represses interferon-stimulated genes. Competition between TASOR and TASOR2 for the shared subunits MPP8 and Periphilin couples retroelement silencing to the immune response.

Danac et al., 2024, Molecular Cell *84*, 1–12
August 8, 2024
https://doi.org/10.1016/j.molcel.2024.06.020

CellPress

Molecular Cell

CellPress
OPEN ACCESS

Article

Competition between two HUSH complexes orchestrates the immune response to retroelement invasion

Joshua Miguel C. Danac,[1,2] Rachael E. Matthews,[1,2,5] Akhila Gungi,[1,2,5] Chuyan Qin,[1,2] Harriet Parsons,[3] Robin Antrobus,[3] Richard T. Timms,[4] and Iva A. Tchasovnikarova[1,2,6,*]

[1]The Gurdon Institute, University of Cambridge, Tennis Court Road, Cambridge CB2 1QN, UK
[2]Department of Biochemistry, University of Cambridge, Tennis Court Road, Cambridge CB2 1QN, UK
[3]Department of Medicine, Cambridge Institute for Medical Research, Addenbrooke's Hospital, Hills Road, Cambridge CB2 0XY, UK
[4]Cambridge Institute of Therapeutic Immunology and Infectious Disease, Jeffrey Cheah Biomedical Centre, Cambridge CB2 0AW, UK
[5]These authors contributed equally
[6]Lead contact
*Correspondence: it257@cam.ac.uk
https://doi.org/10.1016/j.molcel.2024.06.020

SUMMARY

The human silencing hub (HUSH) preserves genome integrity through the epigenetic repression of invasive genetic elements. However, despite our understanding of HUSH as an obligate complex of three subunits, only loss of MPP8 or Periphilin, but not TASOR, triggers interferon signaling following derepression of endogenous retroelements. Here, we resolve this paradox by characterizing a second HUSH complex that shares MPP8 and Periphilin but assembles around TASOR2, an uncharacterized paralog of TASOR. Whereas HUSH represses LINE-1 retroelements marked by the repressive histone modification H3K9me3, HUSH2 is recruited by the transcription factor IRF2 to repress interferon-stimulated genes. Mechanistically, HUSH-mediated retroelement silencing sequesters the limited pool of the shared subunits MPP8 and Periphilin, preventing TASOR2 from forming HUSH2 complexes and hence relieving the HUSH2-mediated repression of interferon-stimulated genes. Thus, competition between two HUSH complexes intertwines retroelement silencing with the induction of an immune response, coupling epigenetic and immune aspects of genome defense.

INTRODUCTION

Mobile genetic elements, such as retroviruses and transposable elements (TEs), threaten the integrity and stability of the genome.[1] The human silencing hub (HUSH) complex constitutes an epigenetic mechanism of defense against invasive genetic elements.[2] HUSH comprises three obligate subunits: TASOR, MPP8, and Periphilin.[3] TASOR acts as a central scaffold that recruits MPP8,[4] a chromodomain-containing protein that recognizes the repressive histone modification H3K9me3,[5,6] and Periphilin, an intrinsically disordered protein that binds nascent RNA from actively transcribed genes.[7,8] Although HUSH can silence exogenous retroviruses[9,10] and synthetic transgenes,[3,7] its primary genomic targets are considered to be evolutionary young LINE-1 (L1) retroelements that are still capable of transposition[11,12] and the long terminal exons of Krüppel-associated box-zinc-finger protein (KRAB-ZNF) genes.[3] How HUSH identifies its target loci remains unclear, but a critical feature appears to be the presence of long transcriptional units devoid of introns.[7] Mechanistically, transcriptional silencing is achieved through the recruitment of the chromatin remodeler MORC2[13] and the H3K9 methyltransferase SETDB1,[3] which together establish a heterochromatic environment. The importance of HUSH-mediated genome defense is underscored by the discovery of viral antagonism of this pathway, with the HIV-2 accessory protein Vpx targeting TASOR for proteasomal degradation.[14,15]

A second line of defense against invasive retroelements is the induction of an immune response. Recognition of retroelement-derived double-stranded RNA (dsRNA) by the pattern recognition receptors (PRRs) melanoma differentiation-associated protein 5 (MDA-5) and retinoic acid-inducible gene I (RIG-I) triggers an innate immune response by inducing interferon (IFN) signaling,[16,17] potentiating the presentation of retroelement-derived antigens on major histocompatibility complex class I (MHC class I) molecules to promote an adaptive immune response.[18] Indeed, the derepression of TEs that follows ablation of HUSH-mediated silencing is thought to trigger IFN signaling.[19] However, despite our understanding of HUSH as an obligate TASOR-MPP8-Periphilin complex,[3,4] only loss of

Please cite this article in press as: Danac et al., Competition between two HUSH complexes orchestrates the immune response to retroelement invasion, Molecular Cell (2024), https://doi.org/10.1016/j.molcel.2024.06.020

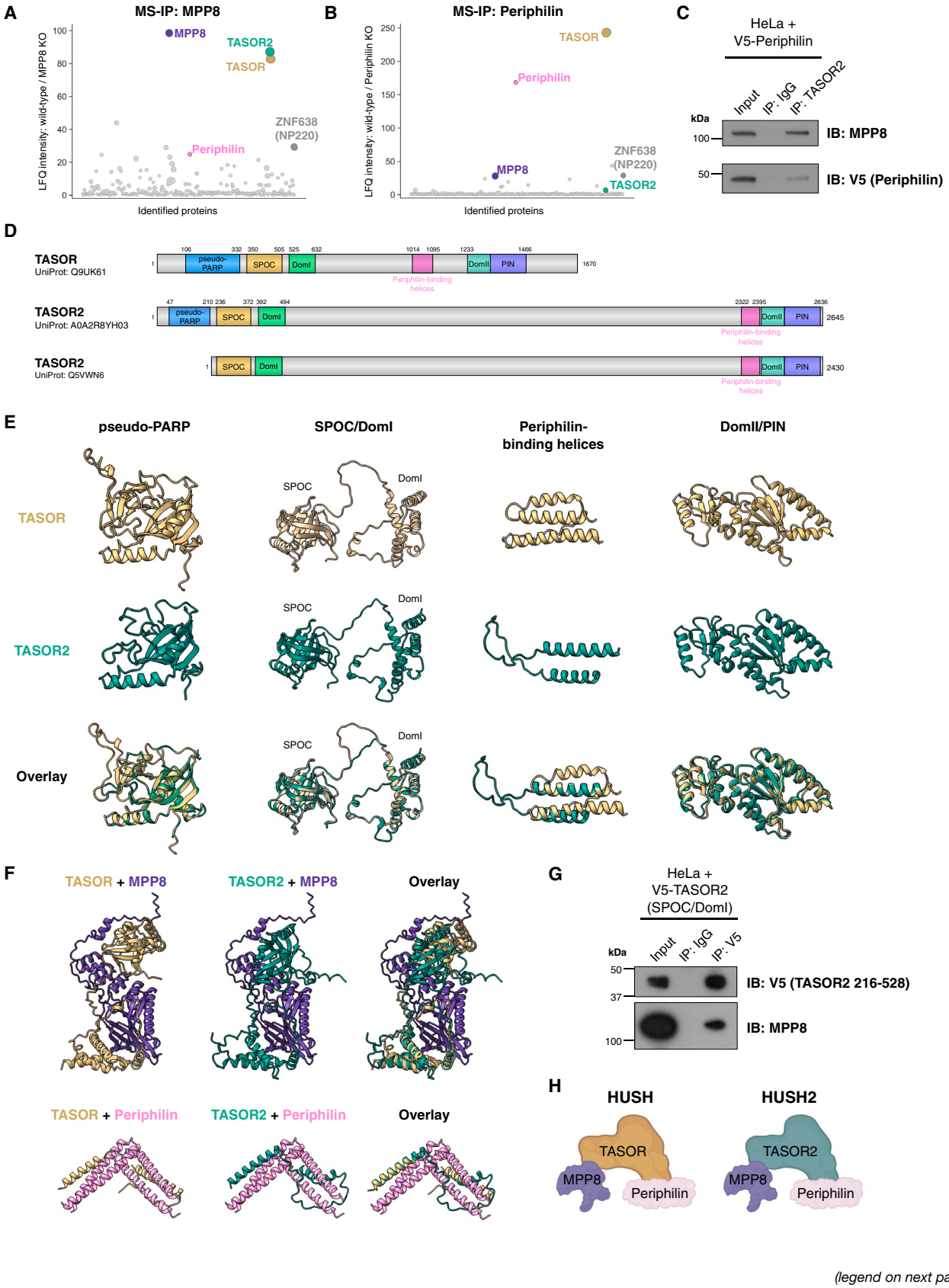

(legend on next page)

MPP8 or Periphilin—but not TASOR—induces an IFN response.[19] The discordance between these phenotypes suggests an unappreciated role for MPP8 and Periphilin outside of the canonical HUSH complex.

Here, we reconcile these observations by identifying a second HUSH complex organized by TASOR2, an uncharacterized paralog of TASOR. The domain architecture of TASOR2 is similar to that of TASOR, and structural modeling predicts that it engages MPP8 and Periphilin in an analogous manner. Unexpectedly, we find that HUSH2 localizes to the promoters of interferon-stimulated genes (ISGs), where it acts as a repressor. As a result of competition between TASOR and TASOR2 for the shared subunits MPP8 and Periphilin, increased demand for HUSH-mediated silencing restricts the assembly of HUSH2 complexes and hence relieves the repression of ISGs. Thus, interplay between HUSH and HUSH2 couples the recognition and silencing of foreign genetic elements with the induction of an immune response, bridging epigenetic and immune facets of genomic defense against invasive elements.

RESULTS

TASOR2 binds MPP8 and Periphilin to form a HUSH2 complex

To examine potential TASOR-independent functions of the HUSH subunits MPP8 and Periphilin, we sought to identify additional binding partners of both proteins by co-immunoprecipitation. In each case, mass spectrometry analysis of nuclear immunoprecipitates identified the other HUSH complex components, plus known accessory factors such as the zinc finger protein NP220[10] (Figures 1A and 1B; Table S1). Notably, TASOR2, a paralog of TASOR with no known function, was also identified as a high-confidence interactor of both MPP8 and Periphilin (Figures 1A and 1B), and we were readily able to validate interactions between TASOR2, MPP8, and Periphilin by co-immunoprecipitation of endogenous TASOR2 followed by immunoblot (Figure 1C).

TASOR2 is completely uncharacterized. Its domain architecture closely resembles that of TASOR, with the canonical isoform (UniProt: Q5VWN6) comprising SPOC, DomI, and DomII/PIN domains, although its central disordered region is significantly larger (Figure 1D). However, there is also evidence supporting expression of longer TASOR2 isoforms containing an N-terminal pseudo-PARP domain (Figures 1D and S1A–S1C). Structural modeling with AlphaFold2[20] suggests that the TASOR2 domains are likely to adopt three-dimensional structures highly similar to the corresponding domains in TASOR (Figure 1E).

TASOR lies at the heart of the HUSH complex: its SPOC and DomI domains bind MPP8,[4] and a pair of alpha-helices mediate the association with Periphilin.[8] The presence of both of these elements in TASOR2 suggested that TASOR2 might organize an analogous HUSH2 complex, which was strongly supported by AlphaFold-Multimer[21] predictions (Figure 1F). Experimentally, we demonstrated that a construct comprising the TASOR2 SPOC and DomI domains (residues 216–528) pulled down MPP8 (Figure 1G). Furthermore, as is the case for TASOR,[3] depletion of TASOR2 reduced the protein levels of MPP8 and Periphilin (Figure S1D). Altogether, these data suggest that TASOR2 lies at the heart of a paralogous HUSH2 complex, which also comprises MPP8 and Periphilin (Figure 1H).

HUSH2 localizes to the promoters of ISGs

Next, we sought to define the genomic targets of the HUSH2 complex. CUT&RUN analysis of endogenous TASOR2 occupancy in K562 cells identified 346 high-confidence binding sites (Figures 2A, S2A, and S2B; Table S2). Notably, MPP8 and Periphilin colocalized with TASOR2 at these sites (Figures 2A, 2C, S2A, and S2C). TASOR and TASOR2 occupancy was mutually exclusive (Figure S2B): in complete contrast to the broad distribution of TASOR (HUSH) across L1 elements[11] and the terminal exons of KRAB-ZNF genes marked by H3K9me3[3] (Figures 2B and 2C), TASOR2 binding sites were overwhelmingly composed of sharp peaks at gene promoters coated with histone modifications associated with active transcription (Figures 2A–2C, S2D, and S2E).

Analysis of the genes downstream of TASOR2 binding sites revealed dramatic overrepresentation of two functional classes: ISGs and KRAB-ZNF genes (Figures 2D–2F). High-confidence TASOR2 peaks were found at the transcriptional start sites (TSSs) of a variety of genes involved in interferon signaling (*IFI35*, *IRF2*, and *STAT2*), antiviral defense (*IFI6*, *ISG15*, *DDX60L*, *ZC3HAV1*, *TRIM5*, and *SAMD9*), and antigen presentation by MHC class I molecules (*B2M, TAP1*, *TAP2*, *TAPBP*, and *PSMB9*) (Figure 2G and Table S2). TASOR2 was also found at the promoters of KRAB-ZNF genes (Figure 2H and Table S2), the protein products of which also function in genome defense by mediating the sequence-specific recruitment of KAP1 (also known as TRIM28) to diverse TEs.[22] Supporting the notion of a HUSH2 complex, MPP8 and Periphilin binding at TASOR2 sites was diminished in *TASOR2*^{KO} cells (Figures S2A and S2C). Suggesting differential recruitment mechanisms at different classes of HUSH2 targets, Periphilin occupancy was completely lost from TASOR2 sites in *TASOR2*^{KO} cells, whereas MPP8 was

Figure 1. The TASOR paralog TASOR2 binds MPP8 and Periphilin to form a HUSH2 complex

(A–C) TASOR2 binds MPP8 and Periphilin. MPP8 (A) and Periphilin (B) were immunoprecipitated from nuclear lysates of wild-type HeLa cells and analyzed by mass spectrometry; corresponding immunoprecipitations from knockout (KO) cell lines[3] served as controls. Bubble size represents the number of peptides identified in wild-type cells. (C) Reciprocal validation by immunoblot: immunoprecipitation of endogenous TASOR2 pulls down MPP8 and Periphilin. Expression of epitope-tagged Periphilin is necessary as the anti-Periphilin antibody does not recognize its epitope following lysis in IGEPAL.[3]

(D) Predicted domain architectures of TASOR and TASOR2. TASOR2 isoforms both with and without the pseudo-PARP domain are shown.

(E–H) TASOR2 lies at the heart of the HUSH2 complex. (E) Comparative AlphaFold2 structure predictions of the TASOR and TASOR2 domains (see also Figures S1A–S1C). (F) AlphaFold2-Multimer predictions comparing the TASOR-MPP8 and TASOR-Periphilin interfaces with the corresponding TASOR2-MPP8 and TASOR2-Periphilin interfaces. (G) MPP8 co-immunoprecipitates with an epitope-tagged TASOR2 construct comprising the SPOC and DomI domains. (H) Schematic representation of the HUSH and HUSH2 complexes.

Please cite this article in press as: Danac et al., Competition between two HUSH complexes orchestrates the immune response to retroelement invasion, Molecular Cell (2024), https://doi.org/10.1016/j.molcel.2024.06.020

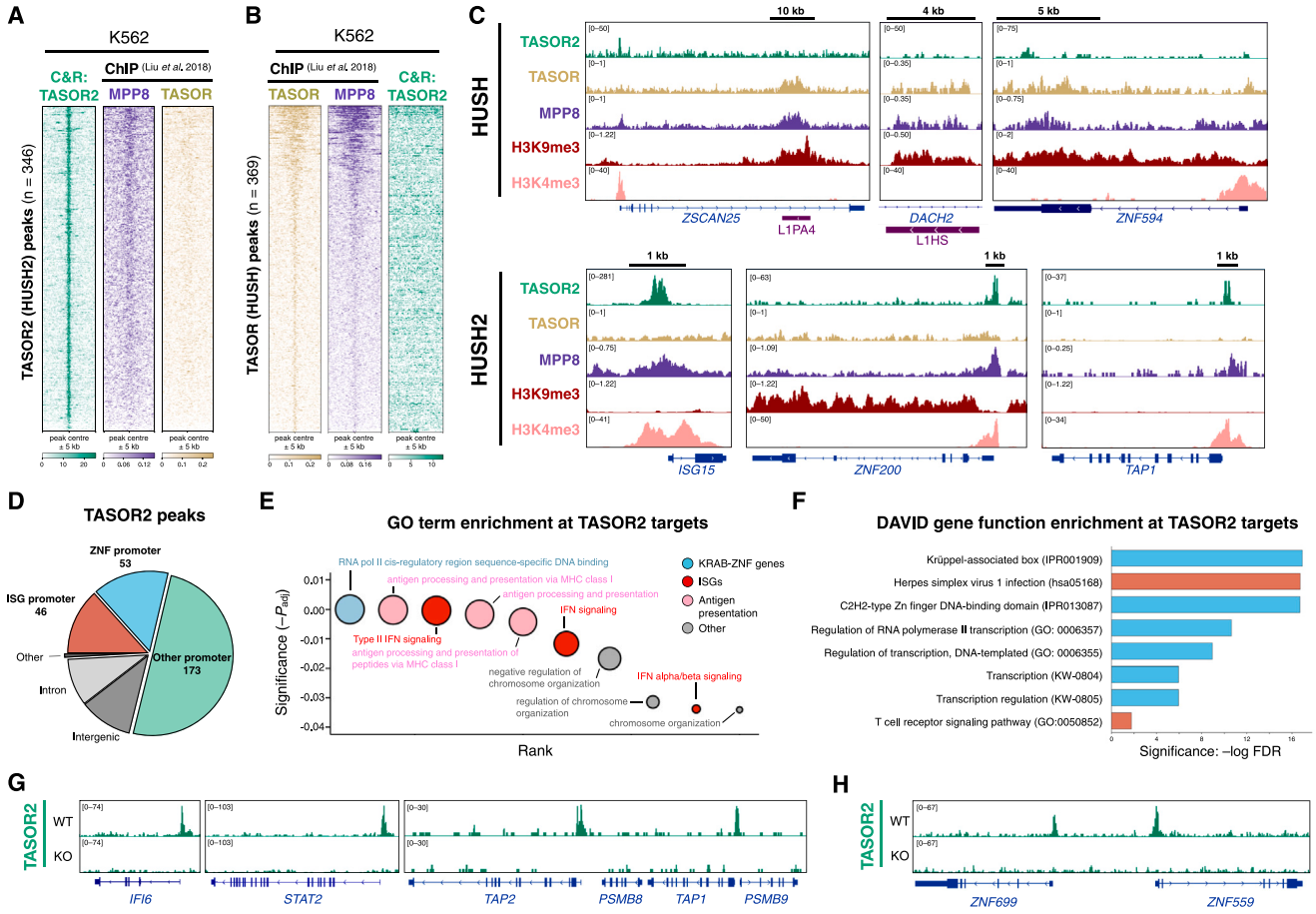

Figure 2. HUSH and HUSH2 occupy distinct genomic sites

(A–C) Defining the genomic localization of HUSH2. CUT&RUN analysis identified 346 high-confidence TASOR2 binding sites in K562 cells, which overlap with MPP8 but not TASOR binding sites determined by ChIP-seq[11] (A). Similarly, TASOR binding sites[11] overlap with MPP8 but not TASOR2 (B). Example loci are shown in (C): TASOR and MPP8 target L1 elements and KRAB-ZNF genes marked by H3K9me3 as part of HUSH, while TASOR2 and MPP8 target gene promoters marked by H3K4me3 as part of HUSH2.

(D–H) HUSH2 binds the promoters of ISGs and KRAB-ZNF genes. The majority of TASOR2 binding sites are found at promoters (defined as within 1 kb of a TSS) (D); the downstream genes are highly enriched for ISGs and KRAB-ZNF genes, as assessed by GO term analysis (E) and DAVID functional gene annotation (F). A range of example ISGs and KRAB-ZNF genes are shown in (G) and (H), respectively.

selectively lost at the majority of ISG targets but not KRAB-ZNF gene promoters (Figures S2F and S2G). Overall, these data demonstrate that TASOR and TASOR2 define two distinct HUSH complexes that share subunit composition but operate at non-overlapping genomic sites.

IRF2 recruits HUSH2 to ISGs

To investigate how HUSH2 localizes to its target sites, we examined the DNA sequence underlying TASOR2 binding sites using motif enrichment analysis. Analysis using the HOMER algorithm[23] identified dramatic enrichment for a set of related interferon-sensitive response element (ISRE) motifs (Figure 3A). ISRE motifs are recognized by transcription factors of the interferon regulatory factor (IRF) family, which raised the possibility that HUSH2 is recruited to ISGs through an interaction with an IRF protein. Intriguingly, the IRF2 consensus site was the most highly enriched motif identified by HOMER (Figure 3A), and large-scale interactome profiling has identified IRF2 as a TASOR2 binding partner in multiple cell lines[24,25] (Figure 3B). Thus, we examined the hypothesis that an interaction between IRF2 and TASOR2 recruits HUSH2 to ISGs.

First, we validated that IRF2 interacts with TASOR2 by co-immunoprecipitation (Figure 3C). Then, using chromatin immunoprecipitation sequencing (ChIP-seq) data from the ENCODE project,[26] we found that IRF2 co-occupies the majority of TASOR2-bound promoters (Figures 3D, S3A, and S3B); however, the IRF2 signal was far stronger across the ISG targets compared with the KRAB-ZNF targets (Figure 3E). Finally, we compared TASOR2 occupancy in wild-type vs. *IRF2*^{KO} cells (Figure S3C) by CUT&RUN. In the absence of IRF2, TASOR2 binding was lost at ISG promoters but not at KRAB-ZNF gene promoters (Figure 3F). Thus, our data suggest that an IRF2-TASOR2 interaction recruits HUSH2 to the promoters of ISGs, whereas an alternative mechanism (potentially via MPP8 as suggested by

Please cite this article in press as: Danac et al., Competition between two HUSH complexes orchestrates the immune response to retroelement invasion, Molecular Cell (2024), https://doi.org/10.1016/j.molcel.2024.06.020

CellPress
OPEN ACCESS

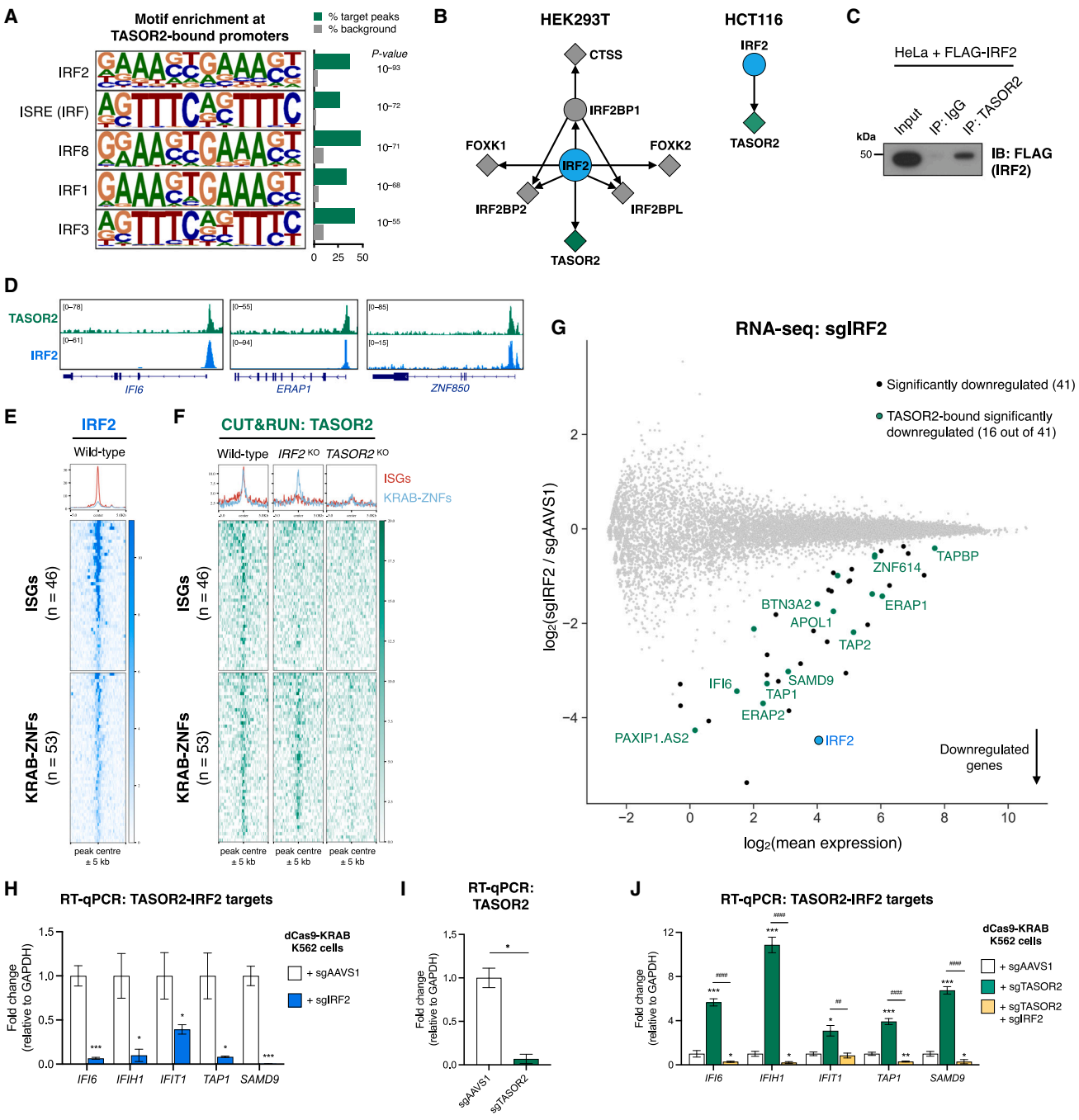

Figure 3. HUSH2 antagonizes IRF2 to repress interferon-stimulated genes

(A) TASOR2 binding sites are enriched for ISRE motifs recognized by IRF-family transcription factors, as assessed by HOMER.[23]

(B and C) TASOR2 binds IRF2. Large-scale interactome profiling[24] identifies a physical interaction between TASOR2 and IRF2 (B), and immunoprecipitation of endogenous TASOR2 pulls down FLAG-tagged IRF2 in HeLa cells (C).

(D–F) IRF2 recruits HUSH2 to the promoters of ISGs. IRF2 co-occupies promoters bound by TASOR2 (D), including ISGs and KRAB-ZNF genes (E). At the promoters of ISGs and KRAB-ZNFs targeted by TASOR2, CUT&RUN analysis in IRF2 knockout cells revealed loss of TASOR2 from ISGs but not KRAB-ZNF genes (F).

(G and H) Loss of IRF2 abrogates expression of ISGs targeted by HUSH2. K562 cells depleted of IRF2 by CRISPRi were analyzed by RNA-seq (G); 41 genes exhibited significant downregulation, 16 of which were bound by TASOR2 (highlighted in green). (H) Individual validation by RT-qPCR, showing mean ± SD of three technical replicates (*$p < 0.05$, ***$p < 0.001$ vs. sgAAVS1; unpaired t tests with Holm-Sidak correction for multiple comparisons).

(I and J) HUSH2 counteracts the IRF2-mediated activation of ISGs. CRISPRi-mediated depletion of TASOR2 (I) results in the derepression of example ISGs as measured by RT-qPCR, but only if IRF2 is present (J). Plots show mean ± SD of three technical replicates (*$p < 0.05$, **$p < 0.01$, ***$p < 0.001$ vs. sgAAVS1 and $^{\#\#}p < 0.01$, $^{\#\#\#\#}p < 0.0001$ vs. sgTASOR2; unpaired t tests with Holm-Sidak correction for multiple comparisons).

the data in Figure S2F) mediates HUSH2 localization to KRAB-ZNF promoters.

HUSH2 counteracts IRF2 to repress ISGs

The localization of TASOR2 to the promoters of ISGs suggested that HUSH2 might cooperate with IRF2 to regulate ISG expression. To interrogate this relationship, we depleted cells of IRF2 by CRISPR interference (CRISPRi) (Figure S3D) and assessed the impact on the transcriptome by RNA sequencing (RNA-seq) (Figure 3G). Consistent with previous studies characterizing IRF2 as a constitutively expressed transcription factor required for basal expression of its target genes,[27,28] loss of IRF2 resulted in significant downregulation of 41 genes (Figure 3G; Table S3), the great majority of which (36/41, 88%) were bona fide ISGs.[29] Intersection with our CUT&RUN data revealed that 16 of the 41 downregulated genes (39%) were bound by TASOR2 (Figure 3G).

Further supporting the notion of a functional relationship between IRF2 and HUSH2, quantitative reverse transcription PCR (RT-qPCR) analysis at example ISGs bound by both TASOR2 and IRF2 revealed that while loss of IRF2 severely reduced ISG expression (Figure 3H), depletion of TASOR2 (Figure 3I) resulted in their upregulation (Figure 3J). This did not occur in cells that were depleted for both TASOR2 and IRF2 (Figure 3J), suggesting that HUSH2 counteracts the IRF2-dependent transcription of these ISGs. Loss of IRF2 did not diminish the expression of KRAB-ZNF genes bound by TASOR2 (Figures S3E and S3F), suggesting that IRF2 is not relevant for HUSH2 function at these sites. Thus, consistent with the notion of HUSH complexes acting as epigenetic repressors, recruitment of HUSH2 to ISGs results in their repression.

Loss of TASOR2, but not TASOR, induces ISG expression

The HUSH complex has previously been suggested to act as a "gatekeeper" of the IFN response: upon abrogation of HUSH function, the resulting derepression of endogenous L1 retrotransposons is postulated to generate dsRNAs, which are sensed by MDA-5 and RIG-I, triggering IFN signaling.[19] However, while genetic ablation of either MPP8 or Periphilin potently induces ISG expression, loss of TASOR has little effect.[19] This observation is difficult to reconcile with the notion that IFN signaling is induced following the transcriptional derepression of repetitive elements, as loss of any HUSH subunit resulted in equivalent activation of L1 expression (Figure S4A), consistent with a range of previous studies.[4,11,12,19,30] By contrast, these data would be fully concordant with a TASOR-independent role for MPP8 and Periphilin in the repression of ISGs as part of HUSH2. Thus, we set out to test the hypothesis that the induction of ISG expression observed upon depletion of MPP8 and Periphilin is not due to impaired HUSH function but rather impaired HUSH2 function.

To do this, we sought to directly compare the functional effects of individual depletion of TASOR, TASOR2, MPP8, and Periphilin on the transcriptome of K562 cells (Figures S4B and S4C). Loss of TASOR resulted in derepression of known HUSH targets, including the clustered KRAB-ZNF[3] and protocadherin[31] genes, but had no effect on ISG expression; by contrast, depletion of TASOR2 upregulated the expression of ISGs and a subset of KRAB-ZNF genes (Figure 4A; Table S4). Indeed, gene set enrichment analysis confirmed an immune response signature in TASOR2-, MPP8-, and Periphilin-depleted cells that was absent from TASOR-depleted cells (Figure 4B). Strikingly, the genes upregulated upon depletion of TASOR or TASOR2 were non-overlapping subsets of the genes upregulated upon depletion of either MPP8 or Periphilin, corresponding to HUSH- and HUSH2-repressed genes, respectively (Figures 4C, 4D, S4D, and S5; Table S5). The upregulated ISGs appeared specific to antiviral defense pathways, including the cytosolic RNA sensors *IFIH1* (encoding MDA-5), *DDX60L*,[32] and *IFIT1*[33] and antiviral factors that restrict RNA viruses (*IFI6*,[34] *SAMD9*,[35] and *OAS3*[36]). TASOR2 was bound to the promoters of these genes (Figure S4E), implicating HUSH2 as a direct repressor of ISG expression. Several upregulated ISGs were also part of the MHC class I antigen presentation pathway (Figure S4F), and, consistent with a specific role for HUSH2 in the repression of ISGs, depletion of either TASOR2, MPP8, or Periphilin—but not TASOR—resulted in increased levels of MHC class I protein expression at the cell surface (Figures S4G and S4H).[37]

Competition between HUSH and HUSH2 couples retrotransposon silencing to ISG induction

With the knowledge that HUSH functions to defend the genome by repressing both exogenous retroviruses and endogenous retrotransposons,[3,11] the finding that HUSH2 represses ISGs and KRAB-ZNF genes—two crucial defense mechanisms against mobile genetic elements—was particularly intriguing. Given that the two HUSH complexes are inextricably linked by virtue of their shared subunits MPP8 and Periphilin, we hypothesized that the cell exploits competition between TASOR and TASOR2 to induce an immune response upon retroviral infection or retrotransposon activity. Specifically, we postulated that an increased requirement for HUSH-mediated genome defense would sequester MPP8 and Periphilin with TASOR, resulting in insufficient MPP8 and Periphilin to assemble HUSH2 complexes with TASOR2 and hence derepression of ISGs. Thus, competition between TASOR and TASOR2 for a limited pool of MPP8 and Periphilin would couple the silencing of invasive genetic elements to the induction of genes involved in the immune response.

We began testing the predictions of this model by manipulating the relative levels of TASOR and TASOR2. Upon deletion of TASOR, CUT&RUN analysis revealed a loss of MPP8 occupancy at HUSH target sites but accumulation at HUSH2 target sites (Figures 5A, 5C, S6A, and S6B), an effect that was recapitulated upon reanalysis of published MPP8 ChIP-seq data in *TASOR*^{KO} cells[11] (Figures 5B and S6C). Similarly, we observed enhanced Periphilin occupancy at HUSH2 sites in *TASOR*^{KO} cells (Figures 5C and S6D). On the other hand, in *TASOR2*^{KO} cells we observed increased MPP8 occupancy at HUSH target sites (Figure S6E), concomitant with decreased MPP8 binding at HUSH2 sites (Figures S2A and S2C). Next, while depletion of TASOR resulted in derepression of L1 elements, loss of TASOR2 resulted in hyper-repression of L1 elements (Figure S6F).[11,38] Lastly, overexpression of TASOR derepressed ISGs targeted by HUSH2 (Figures S6G and S6H), while

Please cite this article in press as: Danac et al., Competition between two HUSH complexes orchestrates the immune response to retroelement invasion, Molecular Cell (2024), https://doi.org/10.1016/j.molcel.2024.06.020

CellPress
OPEN ACCESS

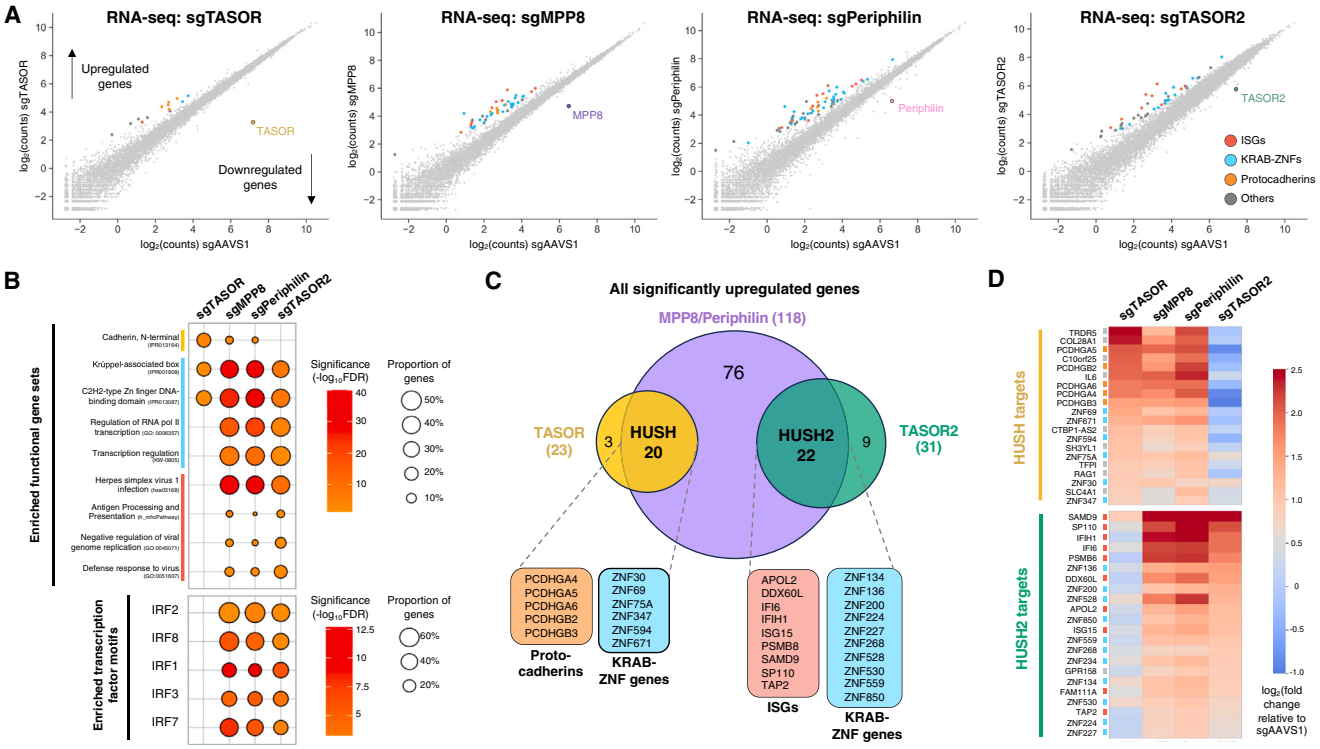

Figure 4. Loss of TASOR2, but not TASOR, induces ISG expression

(A and B) Depletion of TASOR and TASOR2 results in derepression of distinct target genes. (A) Scatterplots summarizing RNA-seq data following CRISPRi-mediated depletion of TASOR, TASOR2, MPP8, or Periphilin in K562 cells; functional groups enriched among the significantly upregulated genes are highlighted. (B) Enrichment analysis of the significantly upregulated genes assessing gene function (top) and transcription factor motifs (bottom) identifies signatures of an immune response upon depletion of TASOR2, MPP8, and Periphilin but not TASOR.

(C and D) Depletion of TASOR and TASOR2 results in derepression of non-overlapping subsets of the genes derepressed upon depletion of either MPP8 or Periphilin. The overlap between the upregulated genes (false discovery rate [FDR] < 0.05, fold change > 1.5) is depicted as a Venn diagram in (C), and the response across each individual HUSH (top) or HUSH2 (bottom) target gene is displayed as a heatmap in (D).

overexpression of TASOR2 upregulated HUSH-repressed L1 elements (Figures S6I and S6J). Furthermore, our model predicts that a stoichiometric excess of MPP8 and Periphilin would relieve the competition between TASOR and TASOR2; indeed, we found both of these effects were rescued by exogenous expression of MPP8 and Periphilin (Figures S6G–S6J). Taken together, these findings suggest an antagonistic relationship between the function of HUSH and HUSH2.

We next examined whether increased retrotransposon activity would relieve HUSH2-mediated repression of ISGs. We reasoned that increased L1 expression would sequester MPP8 and Periphilin into HUSH complexes, preventing the assembly of HUSH2 complexes and thus leading to ISG derepression. In support of this idea, overexpression of a full-length L1PA1 element activated an ISRE-GFP reporter construct in HEK293 cells[19] and resulted in the upregulation of endogenous ISGs in RPE-1 cells.[39] Similarly, we found that exogenous expression of an L1 reporter[7] resulted in the derepression of HUSH2-target ISGs (Figures 5D and 5E) without affecting the expression of TASOR (Figure 5D) or TASOR2 (Figure S6K). Critically, we found that the ISG induction observed upon L1 expression was reversed upon overexpression of exogenous MPP8 and Periphilin (Figures 5D and 5E). Our model also suggests why HIV-2 specifically targets TASOR (rather than MPP8 or Periphilin): not only does Vpx-mediated degradation of TASOR abrogate HUSH-mediated silencing,[14,15] expression of Vpx results in the hyper-repression of HUSH2-regulated ISGs (Figures 5F and 5G). These functional effects reflected changes in TASOR2 occupancy as assessed by CUT&RUN: expression of L1 resulted in loss of TASOR2 from its binding sites, while expression of Vpx enhanced TASOR2 binding (Figures 5H and S6L). Altogether, we propose that HUSH-mediated repression of invasive genetic elements is functionally coupled to the release of ISGs from HUSH2-mediated repression through competition for a limited pool of the shared subunits MPP8 and Periphilin (Figure 6).

DISCUSSION

Here, we identify a second HUSH complex that bridges epigenetic immunity and innate and adaptive immunity, two facets of cellular defense against invasive genetic elements. Despite the similarities between HUSH and HUSH2, which include the shared subunits MPP8 and Periphilin, the extensive structural homology between TASOR and TASOR2, and their common function as epigenetic repressors, these two complexes fulfill starkly different functions. Whereas HUSH represses young L1 elements through the

Please cite this article in press as: Danac et al., Competition between two HUSH complexes orchestrates the immune response to retroelement invasion, Molecular Cell (2024), https://doi.org/10.1016/j.molcel.2024.06.020

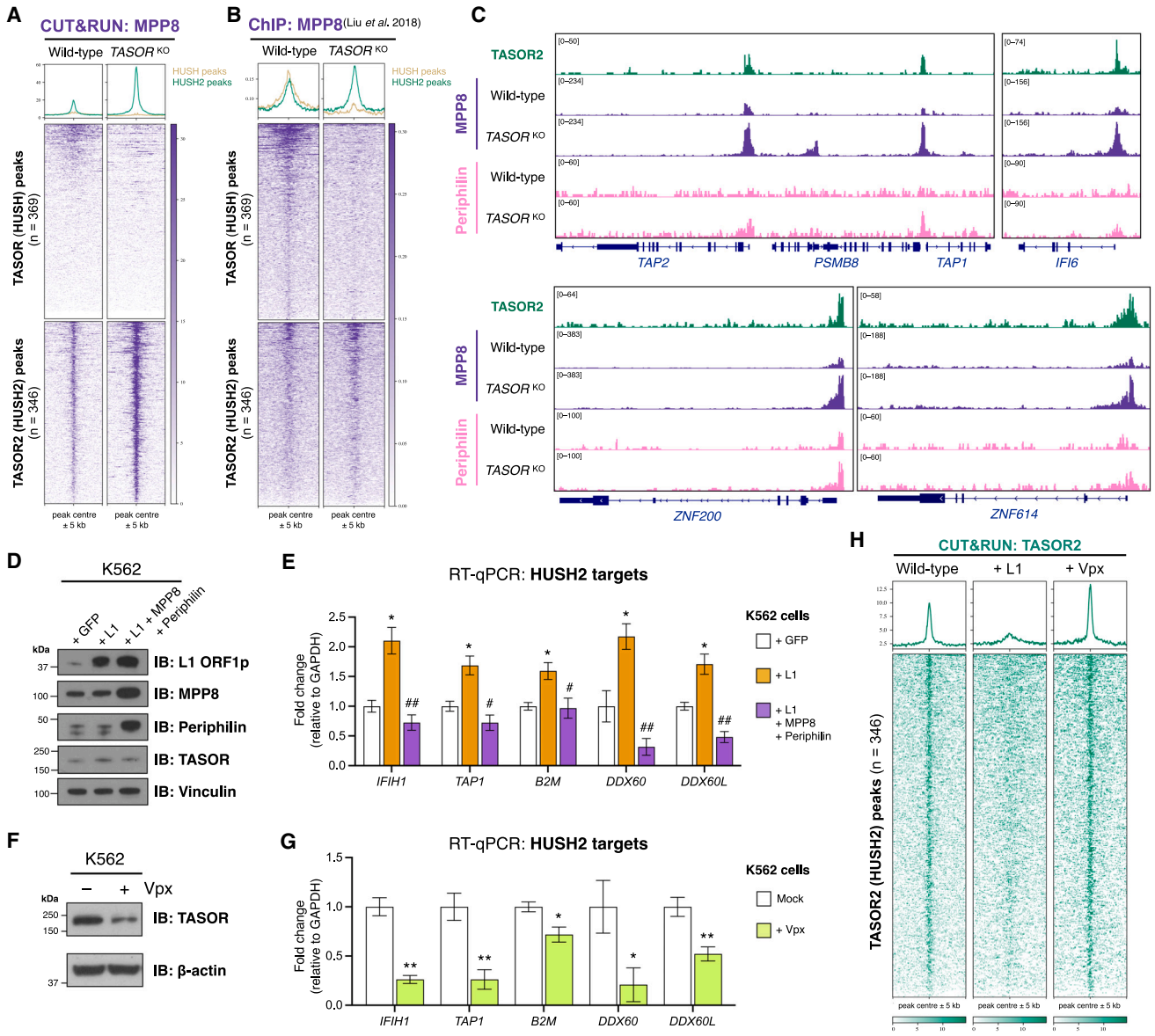

Figure 5. Competition between HUSH and HUSH2 couples retrotransposon silencing to ISG expression

(A–C) Loss of TASOR modulates the occupancy of MPP8 and Periphilin at HUSH2 target sites. MPP8 occupancy increases at HUSH2 target sites in TASOR knockout vs. wild-type K562 cells, as revealed by CUT&RUN (A) and ChIP-seq[11] analysis (B). A range of example loci depicting the accumulation of MPP8 and Periphilin at HUSH2 target sites in TASOR knockout cells by CUT&RUN are shown in (C).

(D and E) L1 overexpression relieves the HUSH2-mediated repression of ISGs. Following exogenous expression of a lentiviral L1 construct in K562 cells (D), RT-qPCR analysis revealed derepression across ISGs targeted by HUSH2 (E); notably, this effect was reversed upon concurrent overexpression of MPP8 and Periphilin. Plots show mean ± SD of three technical replicates (*$p < 0.05$, L1 vs. GFP; $^{\#}p < 0.05$, $^{\#\#}p < 0.01$, L1 + MPP8 + Periphilin vs. L1, unpaired t test with Holm-Sidak correction for multiple comparisons).

(F and G) Vpx-mediated degradation of TASOR (F) results in hyper-repression of ISGs targeted by HUSH2 (G). Plots show mean ± SD of three technical replicates (*$p < 0.05$, **$p < 0.01$ Vpx vs. Mock, unpaired t test with Holm-Sidak correction for multiple comparisons).

(H) The extent of HUSH-mediated silencing determines HUSH2 occupancy at target sites. CUT&RUN analysis of endogenous TASOR2 revealed loss of TASOR2 occupancy upon L1 expression, consistent with MPP8 and Periphilin being diverted to HUSH complexes; conversely, degradation of TASOR via Vpx expression had the opposite effect, enhancing TASOR2 occupancy.

repressive H3K9me3 modification,[3,11] HUSH2 localizes to the promoters of ISGs, where it antagonizes the IRF2-dependent transcription of antiviral response genes. These two roles are intertwined through competition for a limited pool of the shared subunits MPP8 and Periphilin: an increased demand for retroelement silencing tips the balance in favor of HUSH at the expense of HUSH2, ensuring coincident activation of an immune response through the relief of ISG repression.

Please cite this article in press as: Danac et al., Competition between two HUSH complexes orchestrates the immune response to retroelement invasion, Molecular Cell (2024), https://doi.org/10.1016/j.molcel.2024.06.020

CellPress
OPEN ACCESS

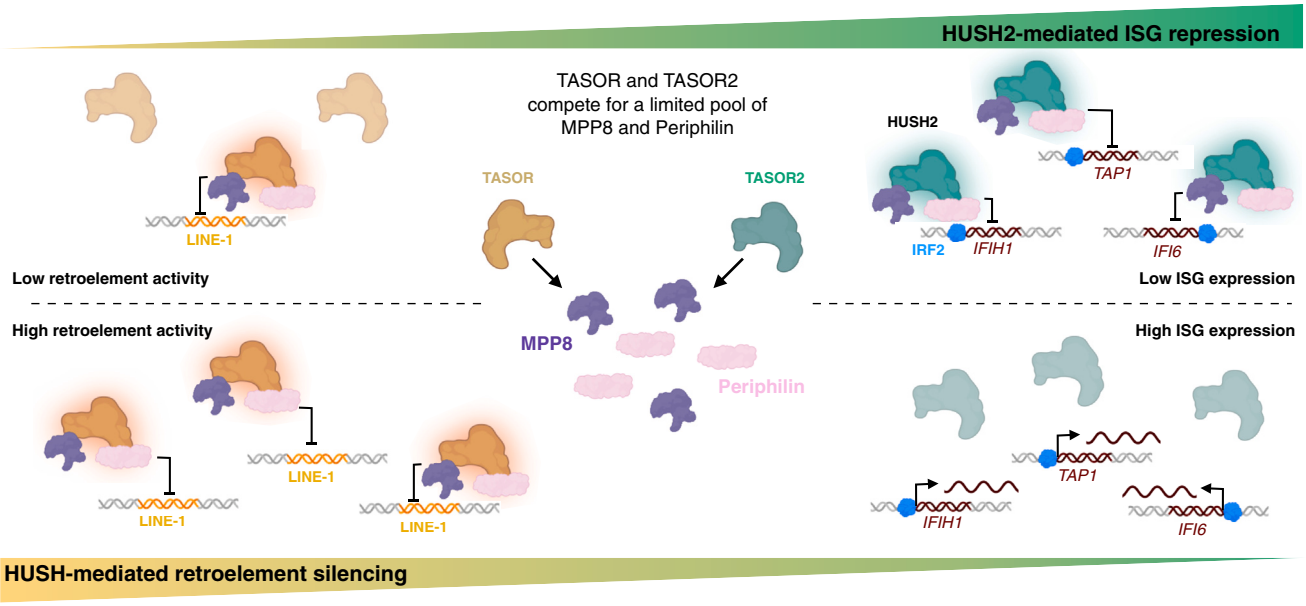

Figure 6. Two competing HUSH complexes couple retroelement silencing to ISG induction

TASOR and TASOR2 compete for a limited pool of MPP8 and Periphilin. When retroelement activity is low, sufficient levels of MPP8 and Periphilin are incorporated into HUSH2 complexes to allow repression of ISGs. A spike in retroelement activity increases the demand for HUSH-mediated silencing, sequestering MPP8 and Periphilin away from HUSH2 complexes and leading to derepression of HUSH2-bound ISGs.

Our findings recontextualize several prior studies demonstrating that the activity of TEs induces innate immune responses.[16,17,19,39–41] Previously, this effect has been attributed to the detection of TE-derived RNAs by the PRRs RIG-I and MDA-5, but here, we show that competition between HUSH and HUSH2 directly couples retroelement sensing to the induction of ISGs. In contrast to classical PRRs, which recognize pathogen associated molecular patterns (PAMPs) and trigger JAK/STAT signaling to activate ISGs,[42] HUSH-mediated silencing directly triggers the induction of ISGs by relieving their repression by HUSH2. It will be interesting to determine the evolutionary origins of TASOR and TASOR2 to assess whether the HUSH-HUSH2 axis could represent a more primitive mechanism to trigger antiviral gene expression in response to retroelement invasion. HUSH and HUSH2 also regulate the expression of KRAB-ZNF genes, which, through their ability to direct the epigenetic repression of TEs in a sequence-specific manner, serve as another arm of the defense response.[22,43]

Recruitment of HUSH to target sites is thought to depend on recognition of the H3K9me3 modification by the MPP8 chromodomain[3,44] and the binding of nascent transcripts by Periphilin.[7,8] As HUSH and HUSH2 target distinct genomic loci, however, it seems unlikely that MPP8 and Periphilin alone drive HUSH localization. For example, we show that IRF2 recruits HUSH2 to the promoters of ISGs but, intriguingly, not the promoters of KRAB-ZNF target genes, while the zinc finger protein NP220 directs HUSH to unintegrated retroviral DNA.[9,10] Thus, we speculate that other as yet unidentified sequence-specific transcription factors will also contribute to the localization of HUSH and HUSH2 to distinct target sites.

How HUSH2-mediated repression is executed remains unclear. Given the absence of H3K9me3 at the promoters of ISGs targeted by HUSH2, it is unlikely that SETDB1 plays a role in prosecuting HUSH2-mediated repression. One possibility is that, like HUSH, HUSH2 cooperates with the nuclear exosome targeting complex (NEXT) to induce degradation of nascent transcripts.[45] Supporting the idea that RNA may play an important role, an interesting parallel between the two HUSH complexes is that, rather than being transcriptionally silenced, their targets maintain a basal level of expression.[4] Thus, future dissection of HUSH2 function may shed light on the molecular mechanisms underpinning epigenetic repression by both HUSH complexes.

HUSH represents an attractive target for therapeutic inhibition. As part of a strategy dubbed "shock and kill,"[46] inhibition of HUSH could serve to purge the persistent pool of latent HIV-1 proviruses that necessitates lifelong antiretroviral therapy to prevent progression to AIDS.[47,48] Alternatively, in the context of cancer immunotherapy, derepression of TEs following inhibition of HUSH could enhance tumor immunogenicity and hence improve the efficacy of immune checkpoint blockade.[16] In each case, our findings suggest that the shared subunits MPP8 and Periphilin may represent the optimal targets, such that derepression of TEs or HIV-1 proviruses upon inhibition of HUSH activity is coupled with enhanced ISG induction and antigen presentation upon inhibition of HUSH2.

Limitations of the study

Our study interrogates the competition between TASOR and TASOR2 in one cell line, K562 chronic myeloid leukemia cells, which are known to exhibit abnormally low levels of L1HS DNA methylation and higher expression of L1.[49] Because L1 expression

is variable across different cell types,[49,50] the precise dynamics of HUSH-HUSH2 competition may also vary. Furthermore, in our HUSH-HUSH2 competition experiments, L1 overexpression was performed using a full-length L1PA1 element driven by the spleen focus-forming virus (SFFV) promoter in place of its native 5′ UTR to facilitate stronger expression; importantly, however, this L1 expression construct is still subject to HUSH-mediated silencing.[7] Finally, in our rescue experiments, we showed that exogenous expression of the shared subunits MPP8 and Periphilin alleviates the competition between TASOR and TASOR2. However, due to the interdependence of HUSH/HUSH2 subunits, we were unable to address the individual contributions of MPP8 and Periphilin.

STAR★METHODS

Detailed methods are provided in the online version of this paper and include the following:

- KEY RESOURCES TABLE
- RESOURCE AVAILABILITY
  - Lead contact
  - Materials availability
  - Data and code availability
- EXPERIMENTAL MODEL AND STUDY PARTICIPANT DETAILS
  - Cell culture
- METHOD DETAILS
  - Generation of lentiviral expression vectors
  - Lentivirus production
  - Generation of knockout cell lines
  - CRISPR interference
  - Co-immunoprecipitation
  - Mass spectrometry analysis
  - Immunoblotting
  - CUT&RUN
  - RT-qPCR
  - RNA-seq
  - Flow cytometry
  - AlphaFold structural prediction
- QUANTIFICATION AND STATISTICAL ANALYSIS
  - Mass spectrometry
  - CUT&RUN
  - ChIP-seq
  - RNA-seq

SUPPLEMENTAL INFORMATION

Supplemental information can be found online at https://doi.org/10.1016/j.molcel.2024.06.020.

ACKNOWLEDGMENTS

We thank Joana Cerveira and her team at the School of Biological Sciences Flow Cytometry Core Facility, Kay Harnish at the Gurdon Institute NGS Facility, and Adam Reid and Ankit Verma at the Gurdon Institute Bioinformatics core. We are grateful to Julie Ahringer for critical reading of the manuscript, Paul Lehner for plasmids, and Emily Naden for helpful discussions. This work was supported by a Cancer Research UK Cambridge Centre studentship to J.M.C.D. and a Pemberton-Trinity fellowship to R.T.T. Research in the Tchasovnikarova laboratory is supported by Wellcome (092096) and Cancer Research UK (C6946/A14492).

AUTHOR CONTRIBUTIONS

Conceptualization, I.A.T.; methodology, J.M.C.D. and I.A.T.; investigation, J.M.C.D., R.E.M., A.G., C.Q., R.T.T., and I.A.T.; formal analysis, J.M.C.D., H.P., R.A., R.T.T., and I.A.T.; writing – original draft, J.M.C.D.; writing – review & editing, J.M.C.D., R.T.T., and I.A.T.; supervision, I.A.T.; funding acquisition, J.M.C.D., R.T.T., and I.A.T.

DECLARATION OF INTERESTS

The authors declare no competing interests.

Received: February 26, 2024
Revised: May 31, 2024
Accepted: June 20, 2024
Published: July 15, 2024

REFERENCES

1. Gázquez-Gutiérrez, A., Witteveldt, J., Heras, S.R., and Macias, S. (2021). Sensing of transposable elements by the antiviral innate immune system. RNA *27*, 735–752. https://doi.org/10.1261/rna.078721.121.
2. Seczynska, M., and Lehner, P.J. (2023). The sound of silence: mechanisms and implications of HUSH complex function. Trends Genet. *39*, 251–267. https://doi.org/10.1016/j.tig.2022.12.005.
3. Tchasovnikarova, I.A., Timms, R.T., Matheson, N.J., Wals, K., Antrobus, R., Göttgens, B., Dougan, G., Dawson, M.A., and Lehner, P.J. (2015). GENE SILENCING. Epigenetic silencing by the HUSH complex mediates position-effect variegation in human cells. Science *348*, 1481–1485. https://doi.org/10.1126/science.aaa7227.
4. Douse, C.H., Tchasovnikarova, I.A., Timms, R.T., Protasio, A.V., Seczynska, M., Prigozhin, D.M., Albecka, A., Wagstaff, J., Williamson, J.C., Freund, S.M.V., et al. (2020). TASOR is a pseudo-PARP that directs HUSH complex assembly and epigenetic transposon control. Nat. Commun. *11*, 4940. https://doi.org/10.1038/s41467-020-18761-6.
5. Kokura, K., Sun, L., Bedford, M.T., and Fang, J. (2010). Methyl-H3K9-binding protein MPP8 mediates E-cadherin gene silencing and promotes tumour cell motility and invasion. EMBO J. *29*, 3673–3687. https://doi.org/10.1038/emboj.2010.239.
6. Li, J., Li, Z., Ruan, J., Xu, C., Tong, Y., Pan, P.W., Tempel, W., Crombet, L., Min, J., and Zang, J. (2011). Structural Basis for Specific Binding of Human MPP8 Chromodomain to Histone H3 Methylated at Lysine 9. PLoS One *6*, e25104. https://doi.org/10.1371/journal.pone.0025104.
7. Seczynska, M., Bloor, S., Cuesta, S.M., and Lehner, P.J. (2022). Genome surveillance by HUSH-mediated silencing of intronless mobile elements. Nature *601*, 440–445. https://doi.org/10.1038/s41586-021-04228-1.
8. Prigozhin, D.M., Douse, C.H., Farleigh, L.E., Albecka, A., Tchasovnikarova, I.A., Timms, R.T., Oda, S.I., Adolf, F., Freund, S.M.V., Maslen, S., et al. (2020). Periphilin self-association underpins epigenetic silencing by the HUSH complex. Nucleic Acids Res. *48*, 10313–10328. https://doi.org/10.1093/nar/gkaa785.
9. Das, A., Vijayan, M., Walton, E.M., Stafford, V.G., Fiflis, D.N., and Asokan, A. (2022). Epigenetic Silencing of Recombinant Adeno-associated Virus Genomes by NP220 and the HUSH Complex. J. Virol. *96*, e0203921. https://doi.org/10.1128/JVI.02039-21.
10. Zhu, Y., Wang, G.Z., Cingöz, O., and Goff, S.P. (2018). NP220 mediates silencing of unintegrated retroviral DNA. Nature *564*, 278–282. https://doi.org/10.1038/s41586-018-0750-6.
11. Liu, N., Lee, C.H., Swigut, T., Grow, E., Gu, B., Bassik, M.C., and Wysocka, J. (2018). Selective silencing of euchromatic L1s revealed by genome-wide screens for L1 regulators. Nature *553*, 228–232. https://doi.org/10.1038/nature25179.
12. Robbez-Masson, L., Tie, C.H.C., Conde, L., Tunbak, H., Husovsky, C., Tchasovnikarova, I.A., Timms, R.T., Herrero, J., Lehner, P.J., and Rowe, H.M. (2018). The HUSH complex cooperates with TRIM28 to repress young retrotransposons and new genes. Genome Res. *28*, 836–845. https://doi.org/10.1101/gr.228171.117.

13. Tchasovnikarova, I.A., Timms, R.T., Douse, C.H., Roberts, R.C., Dougan, G., Kingston, R.E., Modis, Y., and Lehner, P.J. (2017). Hyperactivation of HUSH complex function by Charcot–Marie–Tooth disease mutation in MORC2. Nat. Genet. *49*, 1035–1044. https://doi.org/10.1038/ng.3878.

14. Yurkovetskiy, L., Guney, M.H., Kim, K., Goh, S.L., McCauley, S., Dauphin, A., Diehl, W.E., and Luban, J. (2018). Primate immunodeficiency virus proteins Vpx and Vpr counteract transcriptional repression of proviruses by the HUSH complex. Nat. Microbiol. *3*, 1354–1361. https://doi.org/10.1038/s41564-018-0256-x.

15. Chougui, G., Munir-Matloob, S., Matkovic, R., Martin, M.M., Morel, M., Lahouassa, H., Leduc, M., Ramirez, B.C., Etienne, L., and Margottin-Goguet, F. (2018). HIV-2/SIV viral protein X counteracts HUSH repressor complex. Nat. Microbiol. *3*, 891–897. https://doi.org/10.1038/s41564-018-0179-6.

16. Zhao, K., Du, J., Peng, Y., Li, P., Wang, S., Wang, Y., Hou, J., Kang, J., Zheng, W., Hua, S., et al. (2018). LINE1 contributes to autoimmunity through both RIG-I- and MDA5-mediated RNA sensing pathways. J. Autoimmun. *90*, 105–115. https://doi.org/10.1016/j.jaut.2018.02.007.

17. De Cecco, M., Ito, T., Petrashen, A.P., Elias, A.E., Skvir, N.J., Criscione, S.W., Caligiana, A., Brocculi, G., Adney, E.M., Boeke, J.D., et al. (2019). L1 drives IFN in senescent cells and promotes age-associated inflammation. Nature *566*, 73–78. https://doi.org/10.1038/s41586-018-0784-9.

18. Kong, Y., Rose, C.M., Cass, A.A., Williams, A.G., Darwish, M., Lianoglou, S., Haverty, P.M., Tong, A.-J., Blanchette, C., Albert, M.L., et al. (2019). Transposable element expression in tumors is associated with immune infiltration and increased antigenicity. Nat. Commun. *10*, 5228. https://doi.org/10.1038/s41467-019-13035-2.

19. Tunbak, H., Enriquez-Gasca, R., Tie, C.H.C., Gould, P.A., Mlcochova, P., Gupta, R.K., Fernandes, L., Holt, J., van der Veen, A.G., Giampazolias, E., et al. (2020). The HUSH complex is a gatekeeper of type I interferon through epigenetic regulation of LINE-1s. Nat. Commun. *11*, 5387. https://doi.org/10.1038/s41467-020-19170-5.

20. Jumper, J., Evans, R., Pritzel, A., Green, T., Figurnov, M., Ronneberger, O., Tunyasuvunakool, K., Bates, R., Žídek, A., Potapenko, A., et al. (2021). Highly accurate protein structure prediction with AlphaFold. Nature *596*, 583–589. https://doi.org/10.1038/s41586-021-03819-2.

21. Evans, R., O'Neill, M., Pritzel, A., Antropova, N., Senior, A., Green, T., Žídek, A., Bates, R., Blackwell, S., Jason Yim, J., et al. (2021). Protein complex prediction with AlphaFold-Multimer. Preprint at bioRxiv. https://doi.org/10.1101/2021.10.04.463034v1.

22. Helleboid, P.Y., Heusel, M., Duc, J., Piot, C., Thorball, C.W., Coluccio, A., Pontis, J., Imbeault, M., Turelli, P., Aebersold, R., et al. (2019). The interactome of KRAB zinc finger proteins reveals the evolutionary history of their functional diversification. EMBO J. *38*, e101220. https://doi.org/10.15252/embj.2018101220.

23. Heinz, S., Benner, C., Spann, N., Bertolino, E., Lin, Y.C., Laslo, P., Cheng, J.X., Murre, C., Singh, H., and Glass, C.K. (2010). Simple Combinations of Lineage-Determining Transcription Factors Prime cis-Regulatory Elements Required for Macrophage and B Cell Identities. Mol. Cell *38*, 576–589. https://doi.org/10.1016/j.molcel.2010.05.004.

24. Huttlin, E.L., Bruckner, R.J., Navarrete-Perea, J., Cannon, J.R., Baltier, K., Gebreab, F., Gygi, M.P., Thornock, A., Zarraga, G., Tam, S., et al. (2021). Dual proteome-scale networks reveal cell-specific remodeling of the human interactome. Cell *184*, 3022–3040.e28. https://doi.org/10.1016/j.cell.2021.04.011.

25. Schweppe, D.K., Huttlin, E.L., Harper, J.W., and Gygi, S.P. (2018). BioPlex Display: An Interactive Suite for Large-Scale AP–MS Protein–Protein Interaction Data. J. Proteome Res. *17*, 722–726. https://doi.org/10.1021/acs.jproteome.7b00572.

26. Zhang, J., Lee, D., Dhiman, V., Jiang, P., Xu, J., McGillivray, P., Yang, H., Liu, J., Meyerson, W., Clarke, D., et al. (2020). An integrative ENCODE resource for cancer genomics. Nat. Commun. *11*, 3696. https://doi.org/10.1038/s41467-020-14743-w.

27. Ren, G., Cui, K., Zhang, Z., and Zhao, K. (2015). Division of labor between IRF1 and IRF2 in regulating different stages of transcriptional activation in cellular antiviral activities. Cell Biosci. *5*, 17. https://doi.org/10.1186/s13578-015-0007-0.

28. Kriegsman, B.A., Vangala, P., Chen, B.J., Meraner, P., Brass, A.L., Garber, M., and Rock, K.L. (2019). Frequent Loss of IRF2 in Cancers Leads to Immune Evasion through Decreased MHC Class I Antigen Presentation and Increased PD-L1 Expression. J. Immunol. *203*, 1999–2010. https://doi.org/10.4049/jimmunol.1900475.

29. Rusinova, I., Forster, S., Yu, S., Kannan, A., Masse, M., Cumming, H., Chapman, R., and Hertzog, P.J. (2013). Interferome v2.0: an updated database of annotated interferon-regulated genes. Nucleic Acids Res. *41*, D1040–D1046. https://doi.org/10.1093/nar/gks1215.

30. Zhang, M., Sun, W., You, X., Xu, D., Wang, L., Yang, J., Li, E., and He, S. (2023). LINE-1 repression in Epstein–Barr virus-associated gastric cancer through viral–host genome interaction. Nucleic Acids Res. *51*, 4867–4880. https://doi.org/10.1093/nar/gkad203.

31. Hagelkruys, A., Horrer, M., Taubenschmid-Stowers, J., Kavirayani, A., Novatchkova, M., Orthofer, M., Pai, T.-P., Cikes, D., Zhuk, S., Balmaña, M., et al. (2022). The HUSH complex controls brain architecture and protocadherin fidelity. Sci. Adv. *8*, eabo7247. https://doi.org/10.1126/sciadv.abo7247.

32. Oshiumi, H., Miyashita, M., Okamoto, M., Morioka, Y., Okabe, M., Matsumoto, M., and Seya, T. (2015). DDX60 Is Involved in RIG-I-Dependent and Independent Antiviral Responses, and Its Function Is Attenuated by Virus-Induced EGFR Activation. Cell Rep. *11*, 1193–1207. https://doi.org/10.1016/j.celrep.2015.04.047.

33. Johnson, B., VanBlargan, L.A., Xu, W., White, J.P., Shan, C., Shi, P.-Y., Zhang, R., Adhikari, J., Gross, M.L., Leung, D.W., et al. (2018). Human IFIT3 Modulates IFIT1 RNA Binding Specificity and Protein Stability. Immunity *48*, 487–499.e5. https://doi.org/10.1016/j.immuni.2018.01.014.

34. Richardson, R.B., Ohlson, M.B., Eitson, J.L., Kumar, A., McDougal, M.B., Boys, I.N., Mar, K.B., De La Cruz-Rivera, P.C., Douglas, C., Konopka, G., et al. (2018). A CRISPR screen identifies IFI6 as an ER-resident interferon effector that blocks flavivirus replication. Nat. Microbiol. *3*, 1214–1223. https://doi.org/10.1038/s41564-018-0244-1.

35. Peng, S., Meng, X., Zhang, F., Pathak, P.K., Chaturvedi, J., Coronado, J., Morales, M., Mao, Y., Qian, S.-B., Deng, J., et al. (2022). Structure and function of an effector domain in antiviral factors and tumor suppressors SAMD9 and SAMD9L. Proc. Natl. Acad. Sci. USA *119*, e2116550119. https://doi.org/10.1073/pnas.2116550119.

36. Li, Y., Banerjee, S., Wang, Y., Goldstein, S.A., Dong, B., Gaughan, C., Silverman, R.H., and Weiss, S.R. (2016). Activation of RNase L is dependent on OAS3 expression during infection with diverse human viruses. Proc. Natl. Acad. Sci. USA *113*, 2241–2246. https://doi.org/10.1073/pnas.1519657113.

37. Burr, M.L., Sparbier, C.E., Chan, K.L., Chan, Y.-C., Kersbergen, A., Lam, E.Y.N., Azidis-Yates, E., Vassiliadis, D., Bell, C.C., Gilan, O., et al. (2019). An Evolutionarily Conserved Function of Polycomb Silences the MHC Class I Antigen Presentation Pathway and Enables Immune Evasion in Cancer. Cancer Cell *36*, 385–401.e8. https://doi.org/10.1016/j.ccell.2019.08.008.

38. Li, X., Bie, L., Wang, Y., Hong, Y., Zhou, Z., Fan, Y., Yan, X., Tao, Y., Huang, C., Zhang, Y., et al. (2024). LINE-1 transcription activates long-range gene expression. Published online June 7, 2024. Nat. Genet. https://doi.org/10.1038/s41588-024-01789-5.

39. Ardeljan, D., Steranka, J.P., Liu, C., Li, Z., Taylor, M.S., Payer, L.M., Gorbounov, M., Sarnecki, J.S., Deshpande, V., Hruban, R.H., et al. (2020). Cell fitness screens reveal a conflict between LINE-1 retrotransposition and DNA replication. Nat. Struct. Mol. Biol. *27*, 168–178. https://doi.org/10.1038/s41594-020-0372-1.

40. Gu, Z., Liu, Y., Zhang, Y., Cao, H., Lyu, J., Wang, X., Wylie, A., Newkirk, S.J., Jones, A.E., Lee, M., et al. (2021). Silencing of LINE-1

retrotransposons is a selective dependency of myeloid leukemia. Nat. Genet. *53*, 672–682. https://doi.org/10.1038/s41588-021-00829-8.

41. Simon, M., Van Meter, M., Ablaeva, J., Ke, Z., Gonzalez, R.S., Taguchi, T., De Cecco, M., Leonova, K.I., Kogan, V., Helfand, S.L., et al. (2019). LINE1 Derepression in Aged Wild-Type and SIRT6-Deficient Mice Drives Inflammation. Cell Metab. *29*, 871–885.e5. https://doi.org/10.1016/j.cmet.2019.02.014.
42. Rehwinkel, J., and Gack, M.U. (2020). RIG-I-like receptors: their regulation and roles in RNA sensing. Nat. Rev. Immunol. *20*, 537–551. https://doi.org/10.1038/s41577-020-0288-3.
43. Bruno, M., Mahgoub, M., and Macfarlan, T.S. (2019). The Arms Race Between KRAB-Zinc Finger Proteins and Endogenous Retroelements and Its Impact on Mammals. Annu. Rev. Genet. *53*, 393–416. https://doi.org/10.1146/annurev-genet-112618-043717.
44. Müller, I., Moroni, A.S., Shlyueva, D., Sahadevan, S., Schoof, E.M., Radzisheuskaya, A., Højfeldt, J.W., Tatar, T., Koche, R.P., Huang, C., et al. (2021). MPP8 is essential for sustaining self-renewal of ground-state pluripotent stem cells. Nat. Commun. *12*, 3034. https://doi.org/10.1038/s41467-021-23308-4.
45. Garland, W., Müller, I., Wu, M., Schmid, M., Imamura, K., Rib, L., Sandelin, A., Helin, K., and Jensen, T.H. (2022). Chromatin modifier HUSH co-operates with RNA decay factor NEXT to restrict transposable element expression. Mol. Cell *82*, 1691–1707.e8. https://doi.org/10.1016/j.molcel.2022.03.004.
46. Deeks, S.G. (2012). HIV: Shock and kill. Nature *487*, 439–440. https://doi.org/10.1038/487439a.
47. Armani-Tourret, M., Gao, C., Hartana, C.A., Sun, W., Carrere, L., Vela, L., Hochroth, A., Bellefroid, M., Sbrolla, A., Shea, K., et al. (2024). Selection of epigenetically privileged HIV-1 proviruses during treatment with panobinostat and interferon-α2a. Cell *187*, 1238–1254.e14. https://doi.org/10.1016/j.cell.2024.01.037.
48. Jiang, C., Lian, X., Gao, C., Sun, X., Einkauf, K.B., Chevalier, J.M., Chen, S.M.Y., Hua, S., Rhee, B., Chang, K., et al. (2020). Distinct viral reservoirs in individuals with spontaneous control of HIV-1. Nature *585*, 261–267. https://doi.org/10.1038/s41586-020-2651-8.
49. Philippe, C., Vargas-Landin, D.B., Doucet, A.J., van Essen, D., Vera-Otarola, J., Kuciak, M., Corbin, A., Nigumann, P., and Cristofari, G. (2016). Activation of individual L1 retrotransposon instances is restricted to cell-type dependent permissive loci. eLife *5*, e13926. https://doi.org/10.7554/eLife.13926.
50. Sanchez-Luque, F.J., Kempen, M.-J.H.C., Gerdes, P., Vargas-Landin, D.B., Richardson, S.R., Troskie, R.-L., Jesuadian, J.S., Cheetham, S.W., Carreira, P.E., Salvador-Palomeque, C., et al. (2019). LINE-1 Evasion of Epigenetic Repression in Humans. Mol. Cell *75*, 590–604.e12. https://doi.org/10.1016/j.molcel.2019.05.024.
51. Replogle, J.M., Bonnar, J.L., Pogson, A.N., Liem, C.R., Maier, N.K., Ding, Y., Russell, B.J., Wang, X., Leng, K., Guna, A., et al. (2022). Maximizing CRISPRi efficacy and accessibility with dual-sgRNA libraries and optimal effectors. eLife *11*, e81856. https://doi.org/10.7554/eLife.81856.
52. Tzelepis, K., Koike-Yusa, H., De Braekeleer, E., Li, Y., Metzakopian, E., Dovey, O.M., Mupo, A., Grinkevich, V., Li, M., Mazan, M., et al. (2016). A CRISPR Dropout Screen Identifies Genetic Vulnerabilities and Therapeutic Targets in Acute Myeloid Leukemia. Cell Rep. *17*, 1193–1205. https://doi.org/10.1016/j.celrep.2016.09.079.
53. Brinkman, E.K., and van Steensel, B. (2019). Rapid Quantitative Evaluation of CRISPR Genome Editing by TIDE and TIDER. In CRISPR Gene Editing: Methods and Protocols Methods in Molecular Biology, Y. Luo, ed. (Springer), pp. 29–44. https://doi.org/10.1007/978-1-4939-9170-9_3.
54. Cox, J., and Mann, M. (2008). MaxQuant enables high peptide identification rates, individualized p.p.b.-range mass accuracies and proteome-wide protein quantification. Nat. Biotechnol. *26*, 1367–1372. https://doi.org/10.1038/nbt.1511.
55. Ramírez, F., Ryan, D.P., Grüning, B., Bhardwaj, V., Kilpert, F., Richter, A.S., Heyne, S., Dündar, F., and Manke, T. (2016). deepTools2: a next generation web server for deep-sequencing data analysis. Nucleic Acids Res. *44*, W160–W165. https://doi.org/10.1093/nar/gkw257.
56. Robinson, J.T., Thorvaldsdóttir, H., Winckler, W., Guttman, M., Lander, E.S., Getz, G., and Mesirov, J.P. (2011). Integrative genomics viewer. Nat. Biotechnol. *29*, 24–26. https://doi.org/10.1038/nbt.1754.
57. Kolberg, L., Raudvere, U., Kuzmin, I., Adler, P., Vilo, J., and Peterson, H. (2023). g:Profiler—interoperable web service for functional enrichment analysis and gene identifier mapping (2023 update). Nucleic Acids Res. *51*, W207–W212. https://doi.org/10.1093/nar/gkad347.
58. Sherman, B.T., Hao, M., Qiu, J., Jiao, X., Baseler, M.W., Lane, H.C., Imamichi, T., and Chang, W. (2022). DAVID: a web server for functional enrichment analysis and functional annotation of gene lists (2021 update). Nucleic Acids Res. *50*, W216–W221. https://doi.org/10.1093/nar/gkac194.
59. Quinlan, A.R., and Hall, I.M. (2010). BEDTools: a flexible suite of utilities for comparing genomic features. Bioinformatics *26*, 841–842. https://doi.org/10.1093/bioinformatics/btq033.
60. Mirdita, M., Schütze, K., Moriwaki, Y., Heo, L., Ovchinnikov, S., and Steinegger, M. (2022). ColabFold: making protein folding accessible to all. Nat. Methods *19*, 679–682. https://doi.org/10.1038/s41592-022-01488-1.
61. Pettersen, E.F., Goddard, T.D., Huang, C.C., Meng, E.C., Couch, G.S., Croll, T.I., Morris, J.H., and Ferrin, T.E. (2021). UCSF ChimeraX: Structure visualization for researchers, educators, and developers. Protein Sci. *30*, 70–82. https://doi.org/10.1002/pro.3943.
62. Martin, M. (2011). Cutadapt removes adapter sequences from high-throughput sequencing reads. EMBnet.J. *17*, 10–12. https://doi.org/10.14806/ej.17.1.200.
63. Langmead, B., and Salzberg, S.L. (2012). Fast gapped-read alignment with Bowtie 2. Nat. Methods *9*, 357–359. https://doi.org/10.1038/nmeth.1923.
64. Love, M.I., Huber, W., and Anders, S. (2014). Moderated estimation of fold change and dispersion for RNA-seq data with DESeq2. Genome Biol. *15*, 550. https://doi.org/10.1186/s13059-014-0550-8.
65. Horlbeck, M.A., Gilbert, L.A., Villalta, J.E., Adamson, B., Pak, R.A., Chen, Y., Fields, A.P., Park, C.Y., Corn, J.E., Kampmann, M., et al. (2016). Compact and highly active next-generation libraries for CRISPR-mediated gene repression and activation. eLife *5*, e19760. https://doi.org/10.7554/eLife.19760.

Please cite this article in press as: Danac et al., Competition between two HUSH complexes orchestrates the immune response to retroelement invasion, Molecular Cell (2024), https://doi.org/10.1016/j.molcel.2024.06.020

STAR★METHODS

KEY RESOURCES TABLE

REAGENT or RESOURCE	SOURCE	IDENTIFIER
Antibodies		
Rabbit anti-TASOR	Atlas Antibodies	Cat#HPA006735; RRID:AB_1852384
Rabbit anti-TASOR2	Atlas Antibodies	Cat#HPA038043; RRID:AB_10672402
Rabbit anti-MPP8	Proteintech	Cat#16796-1-AP; RRID:AB_2266644
Rabbit anti-Periphilin	Atlas Antibodies	Cat#HPA038902; RRID:AB_10674844
Rabbit anti-IRF2	Abcam	Cat#ab124744; RRID:AB_10974405
Rabbit anti-ORF1p	Cell Signaling Technology	Cat#88701; RRID:AB_2800129
Mouse anti-β-actin	Sigma-Aldrich	Cat#A2228; RRID:AB_476697
Rabbit anti-Vinculin	Abcam	Cat#ab219649; RRID:AB_2819348
Mouse anti-V5	Abcam	Cat#ab27671; RRID:AB_471093
Mouse anti-FLAG	Sigma-Aldrich	Cat#F1804; RRID:AB_262044
Rabbit IgG isotype control	Cell Signaling Technology	Cat#2729; RRID:AB_1031062
Alexa Fluor 647 anti-human HLA-A,B,C	BioLegend	Cat#311414; RRID:AB_493136
Alexa Fluor 647 Mouse IgG2a, κ Isotype Ctrl	BioLegend	Cat#400234; RRID:AB_2864287
Peroxidase AffiniPure Donkey Anti-Rabbit IgG (H+L)	Jackson ImmunoResearch	Cat#711-035-152; RRID:AB_10015282
Peroxidase AffiniPure Mouse Anti-Rabbit IgG (H+L)	Jackson ImmunoResearch	Cat#715-035-150; RRID:AB_2340770
Bacterial and virus strains		
NEB 5-alpha Competent *E. coli*	New England Biolabs	Cat#C2987
Chemicals, peptides, and recombinant proteins		
PolyJet in vitro DNA transfection reagent	SignaGen Laboratories	Cat#SL100688
Hygromycin B	Thermo Fisher Scientific	Cat#10687010
Blasticidin S HCl	Stratech	Cat#B4879
Puromycin Dihydrochloride	Thermo Fisher Scientific	Cat#A1113803
T4 Polynucleotide Kinase	New England Biolabs	Cat#M0201L
T4 DNA Ligase	New England Biolabs	Cat#M0202L
DNase I	Qiagen	Cat#79256
Pierce Protein A Magnetic Beads	Thermo Fisher Scientific	Cat#88846
Critical commercial assays		
NEBuilder HiFi DNA Assembly Master Mix	New England Biolabs	Cat#E2621
LunaScript RT SuperMix	New England Biolabs	Cat#M3010
Luna Universal qPCR Master Mix	New England Biolabs	Cat#M3003
RNeasy Mini kit	Qiagen	Cat#74106
CUTANA ChIC/CUT&RUN kit	EpiCypher	Cat#14-1048
NEBNext Ultra II DNA Library Prep Kit for Illumina	New England Biolabs	Cat#E7645
NEBNext rRNA Depletion Kit v2	New England Biolabs	Cat#E7405
NEBNext Ultra II Directional RNA Library Prep Kit for Illumina	New England Biolabs	Cat#E7760
Deposited data		
TASOR, MPP8 and H3K9me3 ChIP-seq in K562 cells	Joanna Wysocka laboratory; Liu et al.[11]	GSE95374
IRF2 ChIP-seq in K562 cells	ENCODE	ENCFF102RGH
IRF1 ChIP-seq in K562 cells	ENCODE	ENCFF684EGG
IRF9 ChIP-seq in K562 cells	ENCODE	ENCFF345UOO
H3K4me3 ChIP-seq in K562 cells	ENCODE	ENCFF660WUG

(*Continued on next page*)

Please cite this article in press as: Danac et al., Competition between two HUSH complexes orchestrates the immune response to retroelement invasion, Molecular Cell (2024), https://doi.org/10.1016/j.molcel.2024.06.020

Continued

REAGENT or RESOURCE	SOURCE	IDENTIFIER
H3K9ac ChIP-seq in K562 cells	ENCODE	ENCFF239EBH
H3K27ac ChIP-seq in K562 cells	ENCODE	ENCFF465GBD
Next-generation sequencing data (individual experiments are detailed below)	This manuscript	GSE268799
CUT&RUN for HUSH subunits in wild-type versus *TASOR*^{KO} cells	This manuscript	GSE268794
CUT&RUN for HUSH2 subunits in wild-type versus *TASOR2*^{KO} cells	This manuscript	GSE268795
CUT&RUN for TASOR2 in wild-type versus *IRF2*^{KO} cells	This manuscript	GSE269262
CUT&RUN for TASOR2 in cells expressing L1 or Vpx	This manuscript	GSE268796
TASOR, TASOR2, MPP8 and Periphilin CRISPRi RNA-seq	This manuscript	GSE268797
IRF2 CRISPRi RNA-seq	This manuscript	GSE268798
Experimental models: Cell lines		
K562	ATCC	CCL-243
HeLa	Paul Lehner laboratory; Tchasovnikarova et al.[3]	N/A
HEK293ET	Paul Lehner laboratory; Tchasovnikarova et al.[3]	N/A
Oligonucleotides		
See Table S6	This manuscript	N/A
Recombinant DNA		
pHRSIN-pSFFV-L1-iRFP-WPRE-pSV40-Blasticidin^{R}	Paul Lehner laboratory; Seczynska et al.[7]	N/A
pHRSIN-pSFFV-mCherry-TASOR-WPRE-pPGK-Puromycin^{R}	Paul Lehner laboratory; Douse et al.[4]	N/A
pHRSIN-pSFFV-FLAG-MPP8-WPRE-pPGK-Blasticidin^{R}	Paul Lehner laboratory; Tchasovnikarova et al.[3]	N/A
pHRSIN-pSFFV-V5-Periphilin-WPRE-pPGK-Hygromycin^{R}	Paul Lehner laboratory; Tchasovnikarova et al.[3]	N/A
pHRSIN-pSFFV-GFP-WPRE-pPGK-Hygromycin^{R}	Paul Lehner laboratory; Tchasovnikarova et al.[3]	N/A
pHRSIN-pSFFV-TASOR2(SPOC-DomI)-WPRE-pPGK-Hygromycin^{R}	This manuscript	N/A
pHRSIN-pSFFV-Cas9-WPRE-pPGK-Hygromycin^{R}	Paul Lehner laboratory; Tchasovnikarova et al.[3]	N/A
pHR-UCOE-SFFV-Zim3-dCas9-P2A-Hygro	Marco Jost and Jonathan Weissman; Replogle et al.[51]	Addgene#188768
pHR-pEF1α-ZIM3KRAB-dCas9-P2A-Hygromycin^{R}	This manuscript	N/A
pKLV2-U6-sgRNA-pPGK-Puro-2A-BFP-WPRE	Kosuke Yusa; Tzelepis et al.[52]	Addgene#67974
pKLV2-pSFFV-TASOR-pPGK-Puro-2A-BFP-WPRE	This manuscript	N/A
pKLV2-pSFFV-MPP8-pPGK-Puro-2A-BFP-WPRE	This manuscript	N/A
pKLV2-pSFFV-Periphilin-pPGK-Puro-2A-BFP-WPRE	This manuscript	N/A
pKLV2-pSFFV-TASOR2-V5-NLS-2A-Hygro-WPRE	This manuscript	N/A
pKLV2-pSFFV-FLAG-IRF2-pPGK-Puro-2A-BFP-WPRE	This manuscript	N/A
pHAGE-pRSV-Vpx-IRES-BFP	This manuscript	N/A
Software and algorithms		
TIDE v3.3.0	Brinkman and van Steensel[53]	https://tide.nki.nl
MaxQuant v2.4.13.0	Cox and Mann[54]	https://www.maxquant.org
SeqMonk v1.48.1	Babraham Bioinformatics Group	https://www.bioinformatics.babraham.ac.uk/projects/seqmonk/
HOMER v4.11	Heinz et al.[23]	http://homer.ucsd.edu/homer/motif/

(*Continued on next page*)

Continued

REAGENT or RESOURCE	SOURCE	IDENTIFIER
deepTools v3.5.1	Ramirez et al.[55]	https://deeptools.readthedocs.io/
IGV v2.16.1	Robinson et al.[56]	https://igv.org
g:Profiler	Kolberg et al.[57]	https://biit.cs.ut.ee/gprofiler/gost
DAVID	Sherman et al.[58]	https://david.ncifcrf.gov
Bedtools v2.27.1	Quinlan and Hall[59]	https://bedtools.readthedocs.io/
FlowJo v10.10.0	BD Biosciences	https://www.flowjo.com
ColabFold v1.5.5 (AlphaFold2)	Mirdita et al.[60]	https://colab.research.google.com/github/sokrypton/ColabFold/blob/main/AlphaFold2.ipynb
UCSF ChimeraX v1.6.1	Pettersen et al.[61]	https://www.cgl.ucsf.edu/chimerax/
Cutadapt v1.18	Martin[62]	https://cutadapt.readthedocs.io/
Bowtie2 v2.3.5.1	Langmead and Salzberg[63]	http://bowtie-bio.sourceforge.net/bowtie2/index.shtml
DESeq2	Love et al.[64]	https://doi.org/10.18129/B9.bioc.DESeq2
ggplot2	Hadley Wickham	https://ggplot2.tidyverse.org
Prism v9.5.1	GraphPad	https://www.graphpad.com/

RESOURCE AVAILABILITY

Lead contact

Further information and requests for resources and reagents should be directed to the lead contact, Iva Tchasovnikarova (it257@cam.ac.uk).

Materials availability

Resources generated in this study will be shared by the lead contact upon reasonable request.

Data and code availability

- All sequencing data generated in this study have been deposited to GEO (GSE268799) and are publicly available as of the date of publication. Accession numbers for specific experiments are listed in the key resources table.
- This paper does not report original code. Routine bioinformatics approaches used to analyze the data are described in relevant STAR Methods sections.
- Any additional information required to reanalyze the data reported in this paper is available from the lead contact upon request.

EXPERIMENTAL MODEL AND STUDY PARTICIPANT DETAILS

Cell culture

K562 cells were purchased from ATCC (CCL-243). HeLa cells and HEK293ET cells were a kind gift from Prof. Paul Lehner (CITIID, University of Cambridge, UK). All cell lines were cultured in IMDM supplemented with 10% fetal bovine serum (FBS), penicillin/streptomycin (100 U/ml) and 2 mM glutamine, and were routinely tested for mycoplasma contamination (EZ PCR Mycoplasma Test Kit, Geneflow).

METHOD DETAILS

Generation of lentiviral expression vectors

The lentiviral transfer plasmids pHRSIN-pSFFV-L1-iRFP-WPRE-pSV40-Blasticidin,[7] pHRSIN-pSFFV-mCherry-TASOR-WPRE-pPGK-Puromycin,[4] pHRSIN-pSFFV-FLAG-MPP8-WPRE-pPGK-Blasticidin,[4] pHRSIN-pSFFV-V5-Periphilin-WPRE-pPGK-Hygromycin,[8] pHRSIN-pSFFV-GFP-WPRE-pPGK-Hygromycin[3] and pHRSIN-pSFFV-Cas9-WPRE-pPGK-Hygromycin[13] were generous gifts from Prof. Paul Lehner (CITIID, University of Cambridge, UK). SPOC and DomI domains of TASOR2 (corresponding to residues 216-528 in UniProt A0A2R8YH03) were amplified from HeLa cDNA and cloned in pHRSIN-pSFFV-GFP-WPRE-pPGK-Hygromycin in place of GFP. Full-length TASOR, MPP8 and Periphilin were amplified from the relevant plasmids above, whereas TASOR2 and IRF2 were amplified from K562 cDNA, and cloned into the pKLV2-U6sgRNA-PGKpuro2ABFP-WPRE[52] (Addgene #67974, kindly deposited by Kosuke Yusa) lentiviral vector downstream of an SFFV promoter in place of the U6-sgRNA expression cassette. For CRISPRi,

Please cite this article in press as: Danac et al., Competition between two HUSH complexes orchestrates the immune response to retroelement invasion, Molecular Cell (2024), https://doi.org/10.1016/j.molcel.2024.06.020

the lentiviral expression vector pHR-pEF1α-ZIM3^{KRAB}-dCas9-P2A-Hygromycin was used, which was generated from pHR-UCOE-SFFV-Zim3-dCas9-P2A-Hygro[51] (Addgene #188768, kindly deposited by Marco Jost and Jonathan Weissman). All subcloning steps were performed using the Gibson assembly method (NEBuilder HiFi DNA Assembly Cloning Master Mix, NEB).

Lentivirus production

HEK293ET cells were transfected using PolyJet In Vitro DNA Transfection Reagent (SignaGen Laboratories) with the relevant lentiviral transfer plasmid plus four packaging plasmids encoding Gag-Pol, Rev, Tat and VSV-G respectively. Viral supernatant was harvested 48 hours post-transfection and cell debris removed using a 0.45 μm filter. Target cells were transduced by spinoculation at 800 x *g* for 1 hour. K562 cells were selected with 250 μg/ml hygromycin (ThermoFisher Scientific, #10687010), 10 μg/ml blasticidin (Stratech, #B4879) or 1 μg/ml puromycin (ThermoFisher Scientific, #A1113803) commencing 48 h post-transduction. For co-immunoprecipitation experiments, HeLa cells were selected with 50 μg/ml hygromycin.

Generation of knockout cell lines

Oligonucleotides (IDT) for top and bottom strands of the sgRNA were phosphorylated with T4 PNK (NEB), annealed by heating to 95°C followed by slow cooling to room temperature, and then cloned into the lentiviral sgRNA expression vector pKLV2-U6gRNA5(BbsI)-PGKpuro2ABFP-WPRE[52] (Addgene #67974, kindly deposited by Kosuke Yusa). K562 cells were transduced with pHRSIN-pSFFV-Cas9-pPGK-Hygromycin^R and selected with hygromycin. Following selection, Cas9-expressing cells were transduced with pKLV2-pU6-sgRNA-pPGK-Puro-2A-BFP-WPRE (all sgRNA sequences are listed in Table S6) and selected with puromycin. The resulting population was single cell cloned, and, with the exception of TASOR2, for which there is no available antibody, knockout clones were validated by immunoblot. Successful gene disruption in TASOR2 knockout clones was confirmed by PCR (see Table S6 for primer sequences) and Sanger sequencing (Azenta) followed by TIDE analysis.[53]

CRISPR interference

sgRNA sequences were obtained from the Weissman CRISPRi library[65] (see Table S6 for details). Oligonucleotides (IDT) for top and bottom strands of the sgRNAs were cloned into pKLV2-U6gRNA5(BbsI)-PGKpuro2ABFP-WPRE[52] (Addgene #67974, kindly deposited by Dr. Kosuke Yusa) as described above. K562 cells were transduced with pHRSIN-pSFFV-ZIM3^{KRAB}-dCas9-pPGK-Hygromycin^R and selected with hygromycin. Cells were then transduced with sgRNA expression constructs and selected with puromycin. Successful depletion was verified by RT-qPCR and/or immunoblot.

Co-immunoprecipitation

Cells were washed once in PBS and lysed in cell lysis buffer (0.1% IGEPAL, 10 mM HEPES, 1.5 mM $MgCl_2$, 10 mM KCl plus an EDTA-free protease inhibitor cocktail tablet (Roche)) for 10 min on ice. Nuclear pellets were isolated by centrifugation at 800 x *g* for 5 minutes at 4°C and resuspended in nuclear lysis buffer (1% IGEPAL plus 1:200 Benzonase in TBS). Following removal of insoluble nuclear material by centrifugation (10,000 x *g* for 10 minutes at 4°C), nuclear lysates were pre-cleared with protein A magnetic beads (ThermoFisher Scientific, #88846) for 1 h at 4°C. Immunoprecipitation was performed by incubating the pre-cleared nuclear lysates with 1 μg of antibody and protein A magnetic beads for a minimum of 2 h at 4°C. Co-immunoprecipitates were washed in lysis buffer thrice and eluted by heating at 70°C for 10 min in Laemmli buffer (Bio-Rad, #1610747).

Mass spectrometry analysis

MPP8 and Periphilin co-immunoprecipitations were performed as described above, using ~10^8 wild-type HeLa cells. Polyclonal MPP8 and Periphilin knockout populations[3] served as negative controls. Samples were resolved approximately 1 cm into a pre-cast 4-12% Bis-Tris polyacrylamide gel (ThermoFisher Scientific, #NP0321BOX). The lanes were excised, cut in four equal chunks and the proteins reduced, alkylated, and digested in-gel. The resulting tryptic peptides were analyzed by LC-MS/MS using an LTQ Orbitrap XL coupled to a Waters nanoACQUITY. The nanoACQUITY was operated with solvent A (0.1% formic acid) and solvent B (MeCN, 0.1% formic acid). Peptides were eluted at a flow rate of 250 nl/min using a gradient rising from 8 to 25% solvent B by 27 min then to 40% solvent B by 35 min. MS spectra were acquired in the Orbitrap at 60,000 fwhm resolution with MS/MS spectra acquired in the ion trap. MS/MS spectra were generated by CID fragmentation at 35% NCE in a top6 fashion with fragmented peaks excluded for 45 seconds. Data was processed in MaxQuant 2.4.13.0[54] with carbamidomethylation (C) as a fixed modification and oxidation (M) and acetylation (protein N terminus) as variable modifications. Data was searched against a UniProt human database with LFQ and iBAQ enabled.

Immunoblotting

Cells were washed once in PBS and lysed in whole cell lysis buffer (1% SDS plus 1:200 Benzonase in TBS) for 20 minutes at room temperature. Lysates were then heated to 70°C in Laemmli buffer for 10 min and separated by SDS-PAGE. Proteins were transferred onto PVDF membranes (Merck, #IPFL00010) using a Trans-Blot SD Semi-Dry Transfer Cell (Bio-Rad). Membranes were blocked in 5% milk in PBS + 0.2% Tween-20 and probed overnight with the indicated antibodies at 4°C. Following a minimum of three washes in PBS + 0.2% Tween-20, membranes were incubated with HRP-conjugated secondary antibodies for 40 minutes at room temperature and washed a further three times with PBS + 0.2% Tween-20. Reactive bands were visualized using Pierce ECL Plus Western Blotting Substrate, or SuperSignal West Pico or Dura Chemiluminescent Substrates (ThermoFisher Scientific).

CUT&RUN

CUT&RUN was performed in 5x10^5 K562 cells using the CUTANA CUT&RUN kit (EpiCypher, #14-1048) following the manufacturer's instructions. Targets were enriched using 0.05 μg of primary antibody (see key resources table). Multiplexed sequencing libraries were prepared using the NEBNext Ultra II DNA Library Prep Kit for Illumina (NEB, #E7645), and 61 bp paired-end reads generated on an Illumina NovaSeq 6000 instrument.

RT-qPCR

Total RNA was extracted using the RNeasy kit (Qiagen, #74106) and genomic DNA was removed through on-column DNaseI (Qiagen, #79256) digestion. RNA was converted to cDNA using the LunaScript RT SuperMix (NEB, M3010) and qPCR was performed on a StepOne Real-Time PCR System (ThermoFisher Scientific) using the Luna Universal qPCR Master Mix (NEB, #M3003). Each step was performed as recommended by the manufacturer's protocols. Primer sequences are listed in Table S6.

RNA-seq

Total RNA was extracted using the RNeasy kit (Qiagen, #74106) and genomic DNA was removed through on-column DNaseI (Qiagen, #79256) digestion. Ribosomal RNA was depleted using the NEBNext rRNA Depletion Kit v2 (NEB, #E7405). Multiplexed sequencing libraries were prepared using the NEBNext Ultra II Directional RNA Library Prep Kit for Illumina (NEB, #E7760), and 61 bp paired-end reads were generated on an Illumina NovaSeq 6000 instrument.

Flow cytometry

K562 cells were washed once in PBS and incubated with the relevant antibodies (diluted 1:100 in PBS) for 15 min at 4°C. Following an additional PBS wash, cells were analyzed on a CytoFLEX S instrument (Beckman Coulter) and the resulting data analyzed using FlowJo (BD).

AlphaFold structural prediction

The ColabFold[60] interface was used to perform AlphaFold[2,20] predictions of TASOR and TASOR2 domains, as well as AlphaFold-Multimer[21] modelling of interactions between HUSH and HUSH subunits. Predicted structures were visualized in UCSF ChimeraX.[61]

QUANTIFICATION AND STATISTICAL ANALYSIS

Mass spectrometry

Hits were filtered based on the presence of at least two unique peptides in wild-type cells. Hits were then ranked based on label-free quantification (LFQ) intensity in wild-type cells normalized to knockout controls.

CUT&RUN

Reads were aligned to the human genome (hg38) using Bowtie 2.[63] Peak calling was performed using the implementation of the MACS peak caller in SeqMonk (windows size = 300 bp; $P < 0.00001$). High-confidence TASOR2 peaks were defined as those with a $\log_2$(peak score) > 6. HOMER[23] was used to annotate peaks (*annotatePeaks.pl*) and analyze enriched motifs (*findMotifsGenome.pl*). For visualization, RPKM-normalized bigwig files were generated using deepTools[55] *bamCoverage*. Heatmaps were created using deepTools (*computeMatrix*, *plotHeatmap* and *plotProfile*). Genome browser screenshots were generated using IGV.[56] Gene ontology enrichment analysis was performed using g:Profiler.[57]

ChIP-seq

MPP8, TASOR, and H3K9me3 ChIP-seq data generated by the Wysocka laboratory were downloaded from GEO (GSE95374) and aligned as described.[11] TASOR and MPP8 peaks were called against the signal in their respective knockout cell lines using the MACS2 *callpeak* function (broad peak-calling, $P < 0.001$, fold-enrichment over knockout > 2). High-confidence HUSH peaks were defined by intersecting TASOR and MPP8 peaks using bedtools.[59] The following ENCODE[26] ChIP-seq datasets in K562 cells were used in this study: IRF2 (ENCFF102RGH), IRF1 (ENCFF684EGG), IRF9 (ENCFF345UOO), H3K4me3 (ENCFF660WUG), H3K9ac (ENCFF239EBH), and H3K27ac (ENCFF465GBD). Data was visualized using deepTools and IGV as described above.

RNA-seq

Illumina adaptor sequences were removed with Cutadapt,[62] and the trimmed reads were aligned to the human genome (GRCh38) using Bowtie.[2,63] Uniquely mapped reads with a MAPQ score > 20 were imported into SeqMonk and further analyzed using the RNA-seq quantitation pipeline followed by DESeq2[64] analysis. Enrichment analyses of GO terms and gene functions were performed using g:Profiler[57] and DAVID[58] respectively. Sashimi plots were generated in IGV.[56]